Fluid-Rock Interactions: Lithium Concentrations in Minerals from a block in the Franciscan Complex, California

Sarah Regen

394H

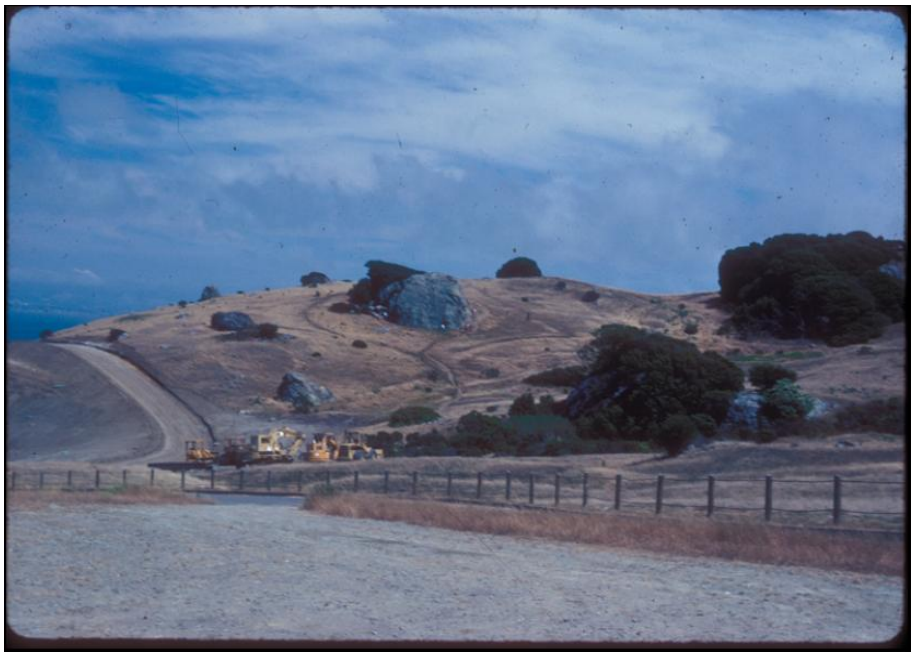

Photo Courtesy of S. Sorensen. Field photo of high-grade blocks from Tiburon, California

Advisors:
Sarah Penniston-Dorland
Philip Piccoli
William McDonough

Table of Contents

Abstract

Concentrations of Li in minerals can help to reveal the amount and degree of interactions between rocks and aqueous fluids. I am studying the Li concentrations of chlorite, amphibole and phengite in a block from the fore-arc thrust of a subduction-setting, which is from a mélange zone of the Franciscan Complex, California in order to decipher the record of fluid-rock interactions experienced by the block. Zoned blocks have interiors that record higher grade metamorphic conditions than the exterior rim. The core minerals are amphibolite facies, whereas blueschist facies dominate the transition zone; the outer rind is a product of metasomatism.

Li concentration differences among core minerals, the reference unaltered phases, the transition zone minerals, accompanying blueschist alteration, and rind minerals are likely to reflect the changing composition of the fluids that have interacted with the rock. Compositional differences in the rind, transition zone, core, and a vein were interpreted as reflecting interactions between rocks and fluids. Whole rock analysis demonstrates that the higher Li concentrations are found in the cores relative to the rind region. Thus, minerals from the core regions should have higher Li concentrations that those in the rinds. In this study, the Li concentrations of amphibole, phengite, and chlorite were measured to see if the patterns observed in the bulk rock were reflected within individual minerals. The results demonstrate that the prediction held true for the most abundant mineral in the rind, amphibole. Phengite grains are extremely heterogeneous, however, and phengites from the different parts of the block overlap in Li concentrations. There was only one grain of chlorite in the rind, and it demonstrated the reverse pattern for what was expected, however the significance of this result is uncertain given the small number of grains.

1. Introduction/Background

"Subduction Factory" is a popular and recent term used to describe the entire system of processes occurring within subduction zones. These processes include the release and transport of fluids in a subduction zone which affects essential earth processes. Many studies have focused on how fluids move through the subduction zone, the sources of the fluids, how the elements are distributed, the degree of alteration of the materials, the material staying in the mantle, and how the inputs into a subduction zone compare to the outputs of the subduction zone and arc volcanic rocks. These studies use a variety of elements as tracers of fluids in subduction zones. One element that has potential for tracing fluids in subduction zones is the element Li, since it is a fluid-mobile element. However, the behavior of Li within a subduction zone is not well understood to date. The Li concentrations in subduction zone rocks can help to better understand the behavior of Li during subduction, how it responds to fluids, and how it partitions in minerals.

1.1 Problem

Are there systematic differences in Li concentrations related with parts of rocks and minerals that have interacted with subduction zone fluids?

Li is expected to partition into fluids during metamorphic dehydration at high pressures and temperatures (Brenan et al., 1998). When fluid is flowing through the subduction zone it is interacting with the rocks. This exchange may be recorded by minerals in subduction zone rocks as they crystallize due to fluid-rock interactions.

1.2 Geologic Background

1.2.1 Mélange Zones

A mélange zone is a large scale, mappable body with rocks of variable size and lithologies in a fine-grained matrix. Mélange zones are found in active continental margins and usually have altered oceanic and continental crust material. Rock types commonly found in mélanges include sedimentary rocks, serpentinite (mantle wedge material), and both metamorphosed and unmetamorphosed oceanic crust. Some of these rock types are found as meter-scale blocks of greywacke, greenstone, and high-grade metamorphic rocks set in a fine-grained matrix (Cloos, 1986; Sorensen et al., 1997; Penniston-Dorland et al., 2010). In subduction zones, mélanges are thought to represent areas of mechanical and metasomatic mixing between a downgoing slab and the overriding mantle wedge (Bebout, 2007). Fluid-rock interactions in these zones can create a metasomatic rind on the outside of the blocks (Cloos, 1986, Sorensen et al., 1997; Bebout 2007; Penniston-Dorland et al., 2010). Evidence for mineral and geochemical alteration of blocks suggests that the mélange zones are regions which have experienced significant fluid flux.

1.2.2 Subduction Zone Metamorphism

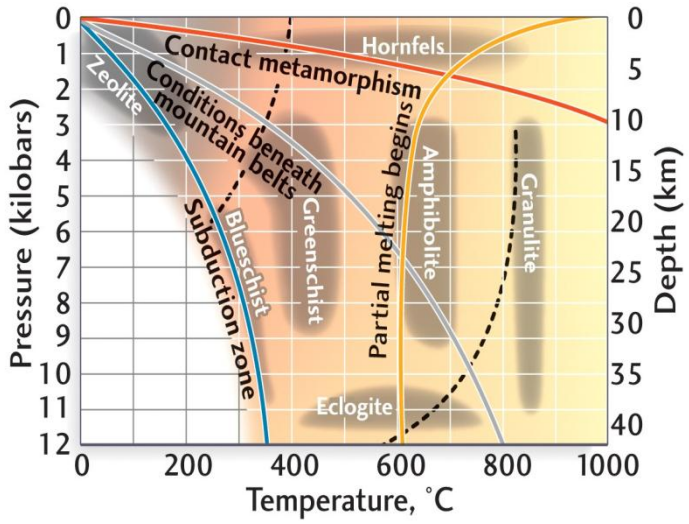

Figure 1: Metamorphic Facies diagram. Adapted from http://hays.outcrop.org/images/rocks/metamorphic/press4e/figure-09-07d.jpg

Metamorphic facies were first described based on mineral assemblages in mafic rocks. Blocks in the Franciscan Complex are in the blueschist, amphibolite, and eclogite facies, suggesting a complex history. Eclogites are products of a high-temperature, high-pressure system. Common mineral assemblages are pyralspite garnet + omphacitic pyroxene (± kyanite ± quartz) and no plagioclase (Winter, 2010). Amphibolites are formed in moderate-temperature, moderate-pressure conditions. The typical mineral assemblage is hornblende + plagioclase (oligoclase, andesine) ± garnet (Winter, 2010). The main facies seen in the Mt. Hamilton block is blueschist. Blueschists are formed in low- temperature, high- pressure systems, which reflect conditions of the subduction process (see figure 1). In hand sample, mafic blueschists are easily recognized by their blue color. The definitive mineral assemblage of this metamorphic facies is glaucophane + lawsonite or epidote/zoisite (± albite ± chlorite ± garnet) (Winter, 2010). The presence of glaucophane and lawsonite is diagnostic and therefore the blueschist facies is characterized by this presence of sodic blue amphiboles that are stable at high temperatures (Winter, 2010).

1.2.3 Franciscan Complex

The Franciscan Complex is an accretionary wedge comprising sediments that were deformed and metamorphosed in an eastward-dipping subduction zone located beneath the western margin of the North American plate from the late Mesozoic to the early Tertiary (Herrington, 1985; Catlos and Sorensen 2003). The mélange zone in the Franciscan has a matrix of fine-grained argillaceous rocks that has been mostly weathered away (Cloos, 1986). This complex is subdivided into three sub-parallel belts; the eastern, the central, and the coastal/western zones (see figure 2). The coastal belt has deformed unmetamorphosed sedimentary rocks (Herrington, 1985). The eastern belt is composed of rocks that are eastward dipping and coherent. The type of rocks generally found in the

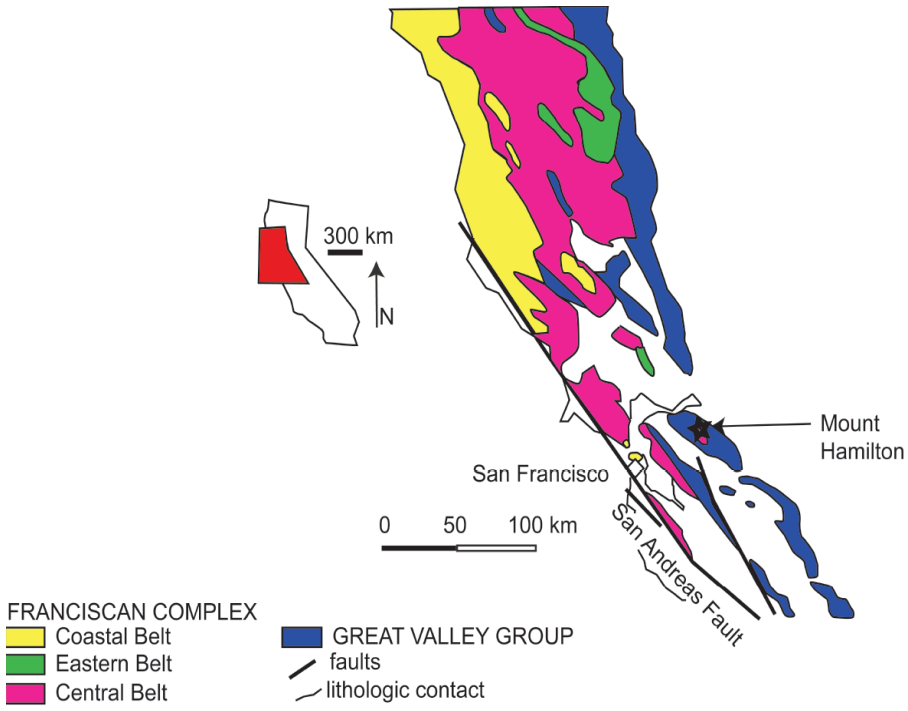

Figure 2: Franciscan Complex and Mt. Hamilton Block Modified by Penniston-Dorland et al., 2010 from Catlos and Sorensen, 2003 and Sorensen et al., 1997.

central belt includes those found in a typical mélange zone as well as cherts and mafic volcanics (Cowan, 1974).

The block being studied is a high-grade, exotic block found adjacent to Kincaid Road, near the intersection with Mt. Hamilton Road. This is in the central mélange belt of the Franciscan complex, located in the Diablo Range in California. The Diablo Range is an anticlinorium with slabs of coherent blueschist facies metasediments and exotic block-bearing mud-matrix mélange (Herrington, 1985). The Franciscan Complex is flanked by the Great Valley Sequence and the Coast Range. The Great Valley Sequence is made of the sediments from the volcanic arc of the Sierra Nevada batholithic belt. These sediments accumulated in the forearc basin (Herrington, 1985). The Coast Range is the crystalline basement of the forearc basin (Herrington, 1985). Subduction ended in the Miocene when the San Andreas Fault formed (Herrington, 1985; Catlos and Sorensen, 2003).

1.2.4 High-Grade Blocks

High-grade blocks found in the Franciscan are roughly ellipsoidal ranging between 1m and 300 m in diameter (Herrington, 1985; Moore and Blake, 1989). Previous workers interpret these blocks to be of basaltic origin (Herrington, 1985, Sorensen et al., 1997). The blocks in the study area are found in metasedimentary and meta-ultramafic matrices that are weathered. The blocks consist of different parts that exhibit different degrees of fluid-related alteration ranging from relatively dry high-grade eclogites to more hydrous low-grade blueschist assemblages and magnesium-rich actinolitic rinds (Herrington, 1985; Giaramita and Sorensen, 1994; Sorensen et al., 1997; Penniston-Dorland et al., 2010). These rinds are usually schistose, with Ca-amphibole ± sheet silicate minerals (Giaramita and Sorensen, 1994). Most Franciscan blocks display evidence for a pre-existing high-pressure, low-temperature block being replaced or overprinted by lower-temperature blueschist mineral assemblages (Cloos, 1986).

1.2.5 Ages of Metamorphism

The high grade blocks, including the Mt. Hamilton block, crystallized during the initiation of subduction of the Farallon plate. The blocks are estimated to be of Late Jurassic to early Cretaceous age (Cloos, 1986; Moore and Blake, 1989; Catlos and Sorensen, 2003). Moore and Blake (1989) estimated ages of 132-155 Ma based on K/Ar dating of primary metamorphic minerals in glaucophane schist, eclogites, and hornblende-rich rocks. Coleman and Lanphere (1971) determined Rb/Sr isotopes on the veins and K/Ar from the phengites estimate an age of 150-153 Ma. The use of a $^{40}Ar/^{39}Ar$ laser on phengite grains demonstrated that they formed when a large ion lithophile element (LILE)-rich fluid altered mid-ocean ridge basalts between 100± 10 Ma and 149± 1 Ma (Catlos and Sorensen, 2003). Based on broad age ranges within different zones of the same phengite grains, the Mount Hamilton blocks are inferred to crystallize over a time period lasting approximately 60 million years. This implies that there were at least 60 Myrs of subduction activity and probably 60 Ma of fluid-rock interactions in the Franciscan Complex (Catlos and Sorensen, 2003).

1.2.6 Pressure and Temperature

Pressure and temperature estimates for the Mt. Hamilton block are based on geothermometry and geobarometry applied to the eclogite and amphibolite interior portions of the study block. Jadeite content of clinopyroxene constrains the prograde pressure to be at least 10.5 ± 1.5 kbar (Giaramita and Sorensen, 1994). The garnet-clinopyroxene thermometer constrains the peak temperatures of 600 – 750°C (Giaramita and Sorensen, 1994).

In general, eclogites of the Franciscan experienced a relatively high-pressure, low-temperature metamorphism (maximum P=10-12 kbar, maximum T= 525-600°C). Amphibolites experienced intermediate pressure, high temperature conditions (P= 9-10 kbar, T=600-700°C). Blueschists experienced a low pressure, low temperature conditions (P=6-7 kbar, T=300-350°C) (Cloos, 1986; Moore and Blake, 1989; Wakabayashi, 1990; Giaramita and Sorensen, 1994; Krogh et al., 1994).

1.2.7 Fluid Flow in Metamorphic Rocks

During subduction, dehydration reactions in the subducted oceanic lithosphere release large quantities of H_2O, which can transport other elements (Sorensen and Grossman, 1989; Bebout and Barton, 1989, 2002). Most of these fluids are likely directed through the mélange zones (Bebout and Barton, 1989, 2002; Breeding et al., 2004). The evidence for the fluids includes dehydrated subduction zone rocks such as eclogites. Rocks that were sitting above the subducting slab in part of their history had some of these fluids passing through them, leaving a trace of their passage behind. Those traces can be observed in fluid inclusions, which provide a way to estimate the pressure and temperature conditions of the interactions (Spear, 1993) in hydrated minerals, in bulk-rock compositions altered by metasomatism (Philpotts and Ague, 2009), in altered stable isotopic compositions, and in altered trace element concentrations.

1.2.8 Fluid-Rock Interactions

The high-grade blocks show evidence of interactions with aqueous fluids (Sorensen et al., 1997; Penniston-Dorland et al., 2010). The following descriptions describe what is interpreted about the fluid interactions in the Franciscan blocks.

At the small scale, there are fluid inclusions in the omphacites and sodic-calcic amphiboles. These inclusions show that low-salinity aqueous fluids were trapped during the eclogite facies metamorphism (Giaramita and Sorensen, 1994). Another line of evidence for fluids is the abundance of hydrous minerals in textural equilibrium with high-grade minerals, for instance sodic amphiboles, epidotes, and phengites (Giaramita and Sorensen, 1994; Penniston-Dorland et al., 2010). Barium zoning patterns within phengite grains suggests that the grains were formed from LILE-rich fluid-rock interactions during subduction metamorphism (Catlos and Sorensen, 2003).

At the large scale, high-pressure, low-temperature metamorphism preserves evidence of subduction zone fluid-rock interactions (Sorensen et al., 1997) such as zoning, hydrous mineral assemblages, and veins formed by high-pressure, low-temperature, hydrous minerals (Giaramita and Sorensen, 1994). There are cavities and veins in the block that are preserved by high fluid pressure during formation and maintained during uplift (Herrington, 1985).

1.2.9 Prograde and Retrograde Fluid Features

Prograde textures that provide evidence for fluids during the peak of subduction zone metamorphism include fluid inclusions in peak metamorphic minerals, hydrous peak metamorphic minerals (phengite), and veins filled with peak metamorphic minerals. Retrograde textures include chlorite replacing garnet, a lower-T amphibole rimming a higher-T amphibole, and low-T hydrous minerals associated with metasomatism in outer part of block.

The combinations of these features are likely to reflect the metamorphic events of these rocks. In the block core there are many fluid inclusions in omphacite, which is a mineral that formed at the peak of metamorphism. Also phengites (which are hydrous) are observed in textural equilibrium with omphacites which are a peak metamorphic mineral.

The blueschist transition zone has several textures suggesting retrograde fluid-rock interactions. There is chlorite (another hydrous mineral) replacing garnet and evidence for growth of amphibole under two different sets of P-T conditions with lower-T sodic amphibole rimming higher-T calcic amphibole.

The block rind is dominated by low-T hydrous minerals, including chlorite and actinolite amphibole. These minerals are associated with metasomatic changes in bulk rock composition, and are thought to be retrograde features.

The vein has hydrous peak metamorphic minerals including garnets and pyroxenes.

1.2.10 Source of Fluids

Evidence suggests that some fluids came from the sediments that were being subducted. The LILE (K, Ba, Rb, and Cs) are all enriched in the rocks, suggesting that the fluids had a sedimentary source (Sorensen et al., 1997). High Li concentration in the block core is consistent with the source of fluid being from subducted sediments (Penniston-Dorland et al., 2010).

1.2.11 Lithium as a Tracer of Fluid Flow

Li is a fluid mobile element, and as such it can used to aid in understanding the fluid events associated with subduction (Penniston-Dorland et al., 2010). Fluid-mobile elements that are readily transported by fluids include LILEs such as K, Ba, Rb, and Cs. Experimental evidence suggests that Li can partition strongly into aqueous fluids at a high pressure and high temperature (Brenan et al., 1998). Previous work on Li in subduction zone metamorphic rocks has emphasized the role of dehydration reactions (Zack et al., 2003), the role of diffusion (Marschall et al., 2007), and the role of fluid infiltration (Penniston-Dorland et al., 2010) in controlling the Li concentrations and isotopic compositions of subduction zone metamorphic rocks.

1.2.12 Lithium Exchange Reactions in Minerals

Li tends to occupy octahedral (6-fold) sites in most silicate minerals, including amphibole, chlorite and phengite, replacing Al or Mg (Wunder et al., 2007). Li has a valence state of +1, and incorporation of Li into a mineral usually involves coupled substitution. This is because of the difference in charge between the Li ion and Mg (+2) and Al (+3). However, Li can also substitute for Na which also has a valence state of +1, and this would be a simple substitution. There are a lot of different coupled substitution mechanisms inferred for Li in amphibole, muscovite, and chlorite. Examples include; in muscovite $^{[6]}Li^{+}$ $^{[6]}Fe^{2+}{}_{-1}$ $^{[4]}Si^{4}{}_{+1}$ $^{[4]}Al^{3+}{}_{-1}$ and $^{[6]}Li^{+}$ $^{[6]}Al^{3+[6]}Fe^{2+}{}_{-2}$ (Brigatti et al., 2001). This is a substitution for Fe bearing muscovites, such as are in the Mt. Hamilton block. Li^{+} may also substitute for K^{+} in the interlayers (Brigatti et al., 2001). In amphiboles Li can substitute into the A or B site (Deer et al., 1991)

Variations in Li concentrations in minerals may reflect variations in Li concentrations in the fluid, however, since more than one element is involved in the incorporation of Li into the mineral structure, these variations might also reflect the activity of other fluid species, such as Si or Al.

1.3 Previous Research

Many studies have been carried out on the Franciscan rocks to understand mineral assemblages, pressure/temperature conditions, and trace element chemistry. Sorensen et al. (1997) focused on whole-rock and phengite geochemistry in eclogites and related rocks

from the Franciscan and Samana Peninsula subduction zone complexes and interpreted the variations of K, Ba, Rb, and Cs (LILE) as being produced by fluid-rock interactions. The study found that based on the relatively high concentrations of the LILE, the source of fluids is likely the dehydration of metasedimentary rocks. Catlos and Sorensen (2003) used Ar and Ba to pinpoint the ages of fluid-rock interactions in the same two paleosubduction zones. They specifically focused on the Ba zoning within phengite grains to select parts of grains from which to obtain $^{40}Ar/^{39}Ar$ ages. This study showed that because of the large difference in ages even within the same grain, the rocks were being metamorphosed for tens of millions of years. Giaramita and Sorensen (1994) reported the occurrences of fluid inclusions in omphacite and sodic-calcic amphiboles in eclogite blocks from the Franciscan. The results of this study suggested that fluids were involved during subduction because the highest grade minerals have fluid inclusions. Moore and Blake (1989) used textural and compositional evidence for an early epidote-amphibolite facies metamorphic event in glaucophane schist and eclogite blocks and concluded that there had to be multiple events of metamorphism. Cloos (1986) reported on the petrologic and structural characteristics of Franciscan and related blueschists. He placed fundamental constraints on tectonic models of the generation and uplift on the blocks. He found that the blocks being studied today were at one point immersed in serpentinite. Herrington (1985) wrote a thesis on the results of petrologic, microprobe, and whole rock analysis of the Mount Hamilton eclogite. The purpose of this paper was to create models on the origin and history of the high-grade blocks. Penniston-Dorland et al. (2010) did a study on high-grade blocks from the Franciscan Complex, California using whole-rock Li concentrations, isotopes, and petrology. The aim of this study was to make sense of fluid-rock interactions in a subduction zone comparing actinolitic rinds and blueschist layers. The outcome of this study found that these blocks have whole-rock Li concentrations higher than the concentrations of pristine mid-ocean ridge basalts (MORB) (ranging from 17 to 39 ppm). The concentrations fall within those found in altered MORB; however the isotopic composition is much lower than expected from altered MORB. Dehydration will lower both the concentrations of Li and the Li isotopic composition, which is not the trend observed for the blocks and rinds, so the observed patterns are therefore interpreted as the infiltration of aqueous fluids.

1.4 Sample Description

1.4.1 Mount Hamilton Sample

The block from Mount Hamilton is approximately 10m in diameter. It is fractured, making it easy to sample the interior zones. The layers sampled are of fresh surfaces as any weathered surface has been cut away with a rock saw. The block consists of several different lithologies and includes an eclogite core with garnet amphibolite regions, a transitional zone with blueschist overprint, coarse-grained veins, and an amphibole-chlorite-phengite rind. Bulk rock compositions of the block are similar to that of ocean floor rocks, suggesting that the blocks were originally mid-ocean ridge basalts (MORB) (Sorensen et al., 1997).

Generally, the concentrations of SiO_2, CaO, Na_2O, and FeO decrease from core to rind. The concentrations of MgO, K_2O, Al_2O_3, and Fe_2O_3 increase from the core to the rind. The

reason for this is consistent with an enrichment of these elements during fluid alteration (Herrington, 1985). Differences in Li concentrations and isotopic compositions between block cores and rinds have been observed as well by Penniston-Dorland et al. (2010). Li concentrations in the rinds are lower than Li concentrations in the block cores. (See figure 3).

The study block exhibits various mineralogical textures that are interpreted as evidence for retrograde, fluid-mediated metamorphic events. These textures include the replacement of omphacite by amphibole, replacement of rutile by titanite, green amphiboles with blue rims, replacement of garnet by chlorite, and an increased abundance of muscovite with no "obvious" replacement of pyroxene or garnet (Herrington, 1985). See textures section for more information.

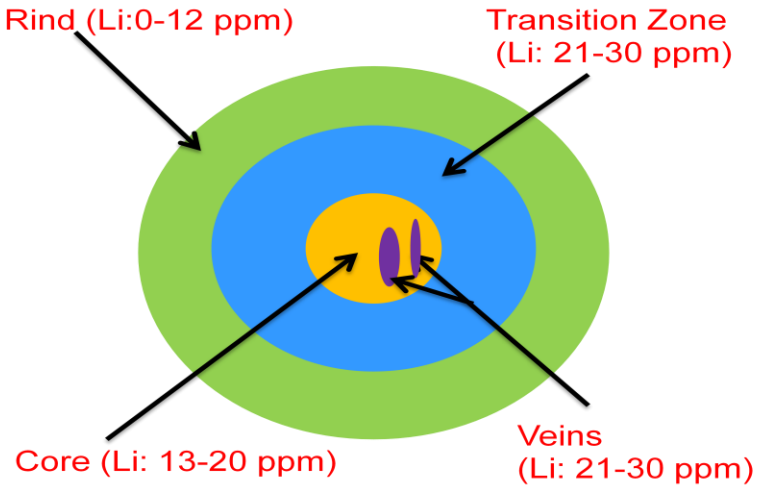

Figure 3: Schematic of Mt.Hamilton block. Li concentrations. (Penniston-Dorland, 2010)

1.4.2 Block Core

The minerals that compose the garnet amphibolite core (MH90-1Aa) are garnet, chlorite, epidote, amphibole, clinopyroxene, titanite, rutile, and muscovite (Sorensen et al., 1997). The core is relatively unaltered, and cavities containing the high-pressure mineral omphacite are preserved which indicate that retrograde alteration and transport to the surface occurred without thoroughly penetrative deformation on the interior of blocks (Cloos, 1986).

1.4.3 Blueschist Transition Zone

The minerals that compose the transition zone (MH90-9) include garnet, chlorite, amphibole, clinopyroxene, titanite, rutile, and muscovite (Sorensen et al., 1997). This zone has completely replaced the original eclogite, is mineralogically distinct, and separates the core from the rind (Herrington, 1985, Sorensen et al., 1997).

1.4.4 Vein

The minerals that compose the vein (MH90-11c) are garnet, chlorite, amphibole, clinopyroxene, titanite, rutile, and muscovite (Sorensen et al., 1997). It is unclear whether the veins were formed at the same time as the eclogite or later.

1.4.5 Rind

The minerals that make up the rind (GL16-4) are coarse-grained amphibole, titanite, rutile, muscovite, chlorite, and zircon (Giaramita and Sorensen, 1994; Sorensen et al., 1997). The rind has higher concentrations of MgO, Cr, and Ni (Sorensen et al., 1997). The Mg-rich rind is thought to be a product of metasomatism by fluids derived from the serpentinization of ultramafic rocks in the matrix (Herrington, 1985; Sorensen et al., 1997). It is not isochemical compared to the block core, and shows evidence for LILE enrichment linked to the retrograde and metamorphic assemblages (Sorensen et al., 1997).

2. Hypothesis

I hypothesize that there have been observable changes in Li concentrations that reflect fluid events in the amphiboles, phengites, and chlorites and that those fluid events produced zoning within these minerals. I expect that Li concentrations of each mineral will be lower in the block rind (GL 16-4) than in the block core (MH90-1Aa). The basis for this hypothesis is measurements in Penniston-Dorland et al. (2010) in which bulk rock Li concentrations in block cores were higher than in block rinds (see figure 1). This study suggests that retrograde fluids have lower Li concentrations than early fluids. Therefore, I also hypothesize that within single minerals Li concentrations will be lower in mineral rims than in the mineral cores. I hypothesize Li zoning based on previous bulk rock studies and from what I can see optically. Optically I have seen retrograde mineral textures resulting from fluid flow and I have seen mineral zoning. Amphiboles in the block generally exhibit zoning with green or brown cores and blue to blue-green rims.

3. Method of Analysis

To complete this study several different methods will be used. Four thin sections were obtained: one each from the rind, the blueschist transition zone, the garnet amphibolite core, and a vein. From each thin section five grains of each mineral were selected. The tools used include the petrographic microscope, the electron probe microanalyzer (EPMA), and the laser ablation inductively coupled plasma mass spectrometer (LA-ICP-MS).

3.1 Petrographic Microscope

The petrographic microscope allows grains to be seen in plane-polarized light, cross-polarized light, and reflected light. Using these different light sources, I have observed zoning, inclusions, retrograde textures, and mapped locations of amphiboles,

chlorites, and phengites. To map the thin sections, the grains being used were documented with a picture taken in all three of the above light sources. In total, five grains of each mineral phase were mapped per thin section.

3.2 Electron Probe Microanalyzer (EPMA)

Amphiboles, chlorites, and phengites were analyzed for their major element composition using a JEOL JXA-8900 Electron Probe Microanalyzer. The EPMA used an accelerating potential of 15 kV, a cup current of 20 nA, and a beam diameter of 10 μm. Raw X-ray intensities were corrected with the ZAF algorithm. The standards used for the amphiboles were Kakanui hornblende, Engels hornblende, rhodonite, and Lake County plagioclase. The standards for the chlorites were albite, Kakanui Hornblende, Engels Hornblende, rhodonite, staurolite, and orthoclase. The standards for the phengites analyses were albite, Kakanui hornblende, Engels hornblende, rhodonite, orthoclase, and hypersthene.

To determine the concentrations of the elements, the number of X-rays emitted by the unknown mineral is compared to the number of X-rays emitted by a primary standard using a wavelength dispersive spectrometer (WDS). Any time there was a question about what a grain might actually be an energy dispersive spectrum (EDS) was done to qualitatively check the composition of the grain.

While using the EPMA, backscattered electron images (BSE) were taken of each study grain, a tool that is appropriate to see some compositional zoning. I marked where each measurement was taken on a BSE image to ensure I used the correct location for the LA-ICP-MS. There were analyses on the cores and rims for each grain. These data were then used to calculate mineral formulas and decipher possible chemical zoning.

3.3 Laser Ablation Inductively Coupled Plasma Mass Spectrometer (LA-ICP-MS)

Trace element compositions of amphiboles, chlorites, and phengites were analyzed in thin section using a single collector ICP-MS (Element 2, Thermo Electron Corp) coupled to a laser ablation system with an output wavelength of 213 nm (UP213, New Wave Research). The laser operated at 2.01 J/cm^2. Laser ablation was done with three, 80μm laser spots per study grain and 7 Hz flash rate. During analysis, data were collected for the following masses: ^{6}Li, ^{7}Li, ^{10}B, ^{11}B, ^{27}Al, ^{29}Si, and ^{43}Ca. Analyses of the two standards were run before and after the study samples. Data was processed with LAMTRACE (Achterbergh et al., 2006) a software program, which determines element concentrations using ratios of count rates for samples and standards, known concentrations in the standards, and the known concentrations of an internal standard in the experimental run products.

The standard reference materials (SRM) for the laser ablation analysis are different from those used for the EPMA. The SRM BCR2g and NIST610 are silicate glasses with known concentrations of Ca, Li, Si, Al and other trace elements (GeoReM). The concentrations of one element, which shows limited variations using the EPMA, was used as an internal standard during the LA-ICP-MS (e.g. Ca in the case of amphiboles, Si for

chlorites and phengites). While the sample is being ablated Li, B, Ca, Al, Si, and other ions are counted. The counts for the element used as an internal standard measured using LA-ICP-MS were compared to the concentrations measured for the same element using the EPMA. This comparison produces a ratio which then can be applied to the measured counts of Li on the LA-ICP-MS resulting in the concentration of Li.

4. Presentation of Data

4.1 Textures

4.1.1 Minerals of Interest

Amphiboles

The general amphibole formula is $A_{0-2}B_2C_5T_8O_{22}$ $(OH)_2$ where the T site is filled with Si and/or Al; the C site has the remaining Al, a ratio of Mg and Fe, and Ti; the B site with Ca, the remaining Mg and Fe, and Na; and the A site is filled with the remaining Na and any K. Trace elements, for example Li, will substitute in the B or C site for Mg or Fe (Deer, et al., 1991). The primary classification of the amphiboles is on the basis of the identity and amounts of the B cations (Hawthorne and Oberti, 2007). This gives four groups of end-members. There is the Mg-Fe-Mn-Li group where $(Ca+Na)_B < 1$ and $(Mg+Fe+Mn+Li)_B \geq 1$. The second grouping is the calcic amphiboles where $(Ca+Na)_B \geq 1$ and $Na_B < 0.5$. The third group is the sodic-calcic group where $(Ca+Na)_B \geq 1$ and $0.5 < Na_B < 1.5$. The fourth group is the sodic amphiboles where $Na_B \geq 1.5$ (Esawi, 2004; Hawthorne and Oberti, 2007). Within each of these groupings, the divisions are based on the Mg/(Mg+Fe) value and amount of Si. Actinolite and tremolite are of the calcic variety and are commonly found in low grade regionally metamorphosed rocks or in low temperature metamorphic conditions (Deer et al., 1992). Glaucophane, a sodium-rich amphibole, is associated with the metamorphism of basaltic rocks is referred to as blueschists (Deer et al., 1992).

Phengites

The general phengite formula is $(K,Ba)(Mg,Fe,Al)_2(Al,Si)_4O_{10}(OH)_2$. By the definition given by the International Mineralogical Association, phengites differ from a white mica by (1) white micas with Si in excess of 3 apfu (atoms per formula unit) in the tetrahedral site and (2) white micas with larger amounts of Fe and Mg (in any oxidation state) and other larger elements such as Ti, Cr, etc. in the octahedral state (Cibin et al., 2008). Phengite is created from muscovite by replacing an Al in both the tetrahedral and octahedral site with Mg and Si (Deer et al., 1992). Phengites are found in rocks in the blueschist facies (Deer et al., 1992).

Chlorites

The general chlorite formula is $(Mg,Fe,Al)_{5-6}(Al,Si)_4O_{10}(OH)_8$. Chlorite is a sheet silicate mineral that has solid solution among Mg, Fe, and Mn. The four various end members are clinochlore $Mg_5Al_2Si_3O_{10}(OH)_8$, daphnite $Fe_5Al_2Si_3O_{10}(0H)_8$, sudoite $Mg_2Al_4Si_3O_{10}(OH)_8$, iron sudoite $Fe_2Al_4Si_3O_{10}(OH)_8$, and Mn-chlorite $Mn_5Al_2Si_3O_{10}(OH)_8$. Clinochlore is found as a hydrothermal alteration product of amphiboles, pyroxenes, and biotite. Daphnite is usually found in sedimentary ironstones from reducing conditions. Sudoite is associated with low

grade assemblages. Fe-sudoite is distinguished from sudoite based on the Fe^{3+} content. Commonly chlorite is found as a retrograde metamorphic alteration product or is from a metasomatic reaction (Anthony et al., 2001).

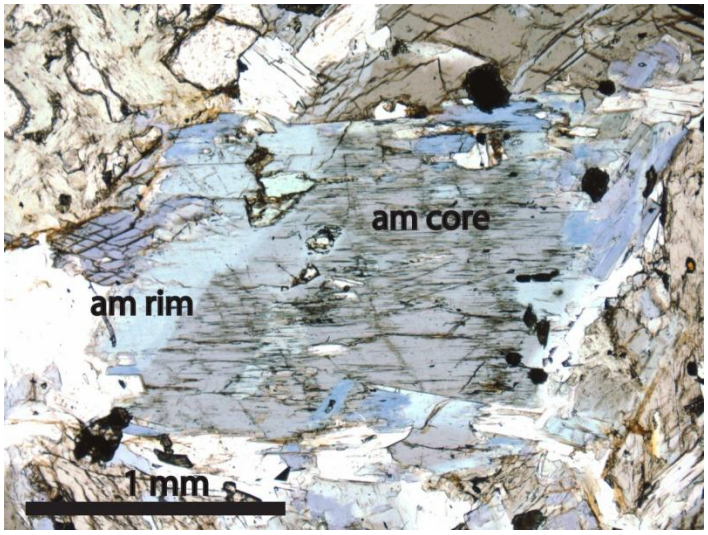

Figure 5 Photomicrograph of sample MH90-1Aa (block core) rimmed amphibole exhibiting brown amphibole core and a blue amphibole rim (5x). am- amphibole

4.1.2 Amphibole

Many of the amphiboles in this block are compositionally zoned. This can be seen when observing the thin sections optically and in some cases by BSE imaging.

Amphiboles are optically zoned with brown, green, or blue amphibole cores and blue rims (Herrington, 1985; Giaramita and Sorensen, 1994). The cores are generally irregular in shape. There are different species of amphiboles that occur throughout the block; edenitic hornblende (brown), barrosite (blue-green), and glaucophane-crossite (blue) (Moore and Blake, 1989; Giaramita and Sorensen, 1994). The grains are tabular to equant and range in size from 2 mm to 5 mm with scattered inclusions of rutile, epidote, and clinopyroxene (Herrington, 1985; Moore and Blake, 1989). There is some replacement of amphibole by chlorite in this sample as well (Moore and Blake, 1989). (See figure 4). One thing to note is that amphibole classifications have changed recently, and the names of the above amphiboles were assigned using a slightly different classification scheme.

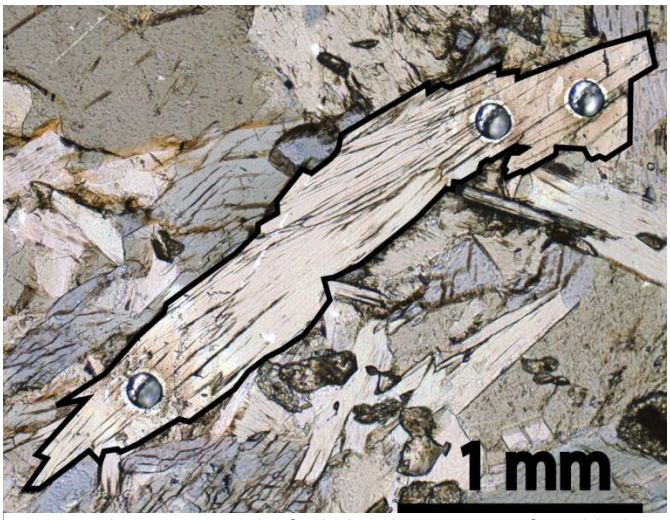

Figure 4: Photomicrograph of tabular phengite grain from block core (10x).

4.1.3 Phengites

Phengites increases in abundance towards the rinds. They are tabular (see figure 5) and are approximately 1-2 mm in length (Herrington, 1985). According to Herrington (1985), there are some chlorite pseudomorphs of phengite. In some places the phengites are broken and in others they are straight and thick.

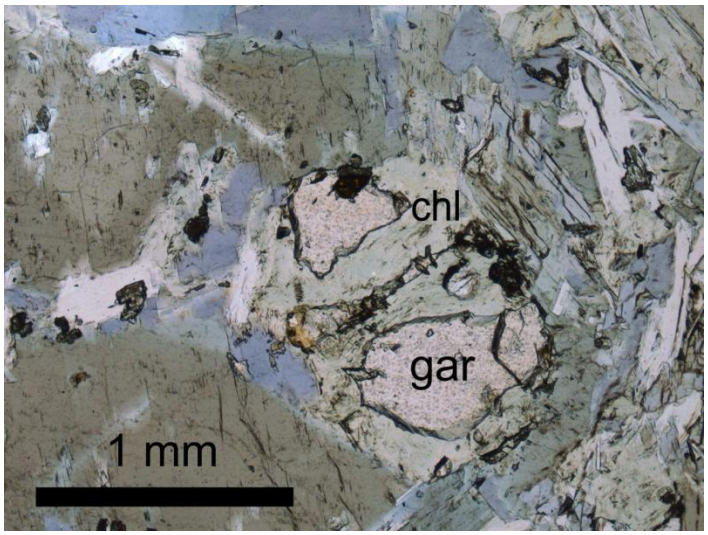

Figure 6: Garnet altered to chlorite from block core (10x). Chl- chlorite gar- garnet

4.1.4 Chlorite

Chlorite is usually found at garnets edges, except in the rind where there is no garnet (see figure 6). In the transition zone, chlorite has completely pseudomorphed the garnets. The chlorites do not necessarily have to be around a garnet. The amount of chlorite decreases outwards in the rind.

4.2 EPMA Data

The first step in data analysis was to check that the total falls within the expected range of totals for the given mineral. All of these minerals are hydrous, and water (OH) content is not measured using the microprobe, so totals are not expected to be 100%. If the totals did not fall within 1.5 wt. % of the range of expected values, then the analysis likely hit a crack or hole in the mineral and the data were not used. For each grain the analyses that are similar are grouped together as a homogenous grain. If there were variation in analyses, the like values are grouped together. The average composition, the average total, and mineral formula unit for amphiboles were calculated and classified following Hawthorn and Oberti (2007) as well as Esawi (2004). The phengites and chlorites were classified following CACLMIN (Brandelik, 2004).

4.2.1 Amphiboles

The amphibole data from the EPMA was plugged into AMPH-CLASS, a spreadsheet by Esawi (2004). This spreadsheet is modeled after the International Mineralogical Associations 1997 amphibole classification. By inputting my values of the oxides (measured from the EPMA) and the number of oxygen's to use (23 in the case of amphiboles) AMPH-CLASS will calculate a mineral formula. It will also calculate the ferric-ferrous content (Esawi, 2004).

When picking amphibole grains, no distinction or preference was made based on type of amphibole or compositional zoning. There is a correlation between the amphibole being sodic, calcic, or sodic calcic and the location of the mineral in the block. The block rind exhibits a calcic composition, composed mostly of actinolite. The transition zone has a mixture of calcic amphiboles as well as sodic amphiboles. The block core is dominated by sodic-calcic amphiboles. Finally, the vein is composed of calcic, sodic, and sodic-calcic amphiboles. Certain minerals only appear in certain parts of the block, for instance; actinolite is only in the block rind, edenite is only in the transition zone, and barroisite in only the vein.

See tables 1-6 in the appendix for electron probe compositions of amphiboles. The classification of the amphibole also follows a pattern within the grains (see table 7 in appendix for amphibole names). The mineral cores in the transition zone are magnesiokatophorites or edenites (more calcic). The mineral rims are glaucophane or winchite (more sodic-rich). The vein has amphiboles with rims that are mostly sodic-calcic and cores that are mostly sodic. There is also a correlation between a certain type of amphibole and its locality within the block. For example, actinolite is only found in the rind, edenite is only in the transition zone, and barroisite only occurs in the vein.

One more pattern is the relatively unaltered block core and the metasomatic block rind both have the least amount of compositionally zoned amphiboles whereas the transition zone and vein mostly exhibit compositional zonation.

4.2.2 Chlorite

The general chlorite formula is $(Mg,Fe,Al)_{5\text{-}6}(Si)_4O_{10}(OH)_8$. By taking the average of all chlorite grains and using CALCMIN to convert the data from oxides to wt % the average Franciscan chlorite formula was calculated. It is $(Mg_{2.92},Fe_{1.76},Al_{1.15})(Al_{.97}Si_{3.03})O_{10}(OH)_{8.}$ The octahedral site is in range of the 5-6 cation value.

There does not seem to be a compositional change from block core to block rind. The wt % oxides after being averaged are within 5% of each other. This is based on the average of the rind chlorites and the core chlorites.

4.2.3 Phengites

The general phengite formula is $(K,Ba)(Mg,Fe,Al)_2(Al,Si)_4O_{10}(OH)_2$. CALCMIN was used to convert the average of the phengite compositions to produce an average Franciscan phengite formula of $(K_{.7}Ba_{.03})(Mg_{.41}Fe_{.06}Al_{1.44})(Al_{.61}Si_{3.39})O_{10}(OH)_2$. There is not a lot of variation in composition within the block for the phengites. The most noticeable differences are in the amount of Cr. There is more Cr in phengites from the block rind than from the block core. This can be attributed to the metasomatism that increases the bulk Cr content of the rind.

4.3 LA-ICP-MS Data

When comparing the average Li concentrations of minerals, the Li increases from the from the block core to the block rind, where the core is lower and the rind is higher, in phengites and chlorites. The amphiboles exhibit the opposite trend (see figure 7).

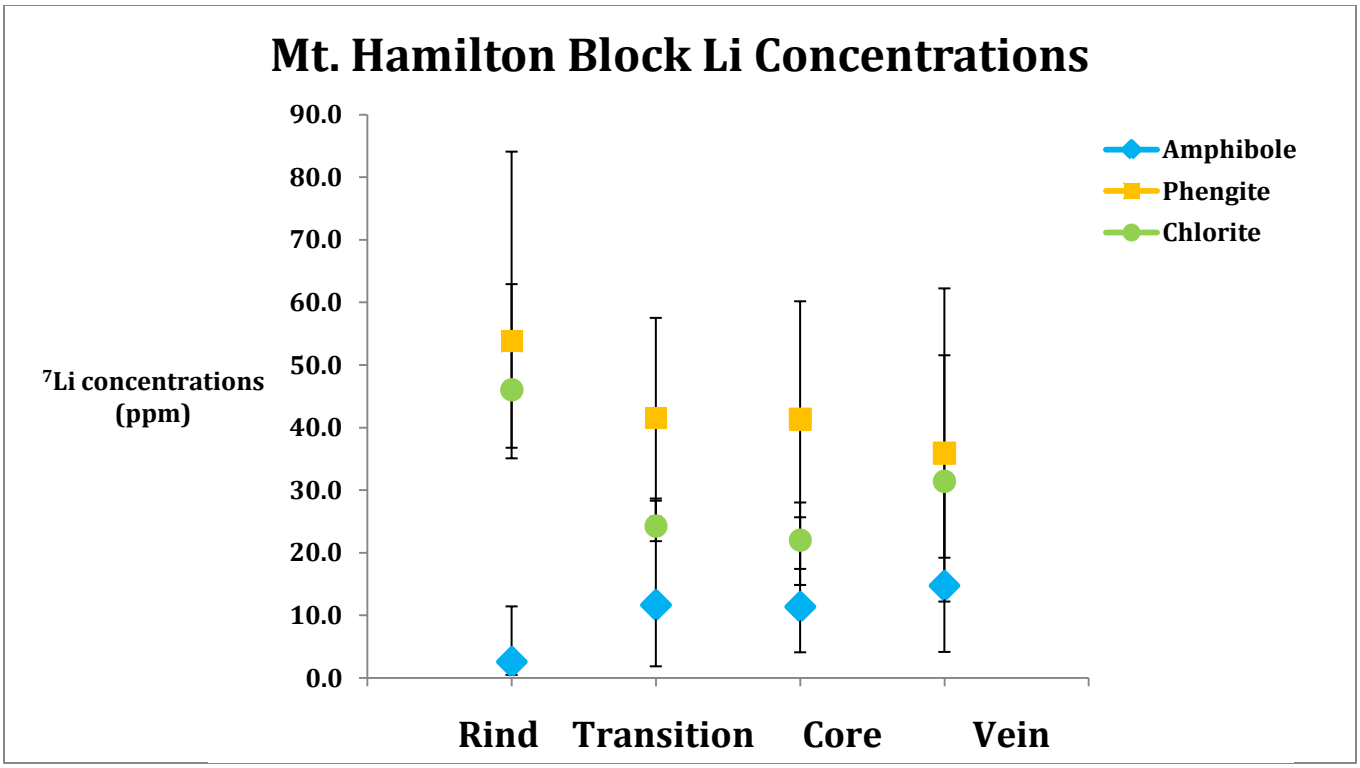

Figure 7: Average Li concentrations with minimum and maximum values

See appendix for average concentrations, ranges, and 2σ of Li in minerals analyzed.

4.3.1 Amphibole

The average amphibole values show a general decrease from the block core to the block rind. The block core has maximum Li values of 28.3 ppm and the block rind has minimum Li values of 0.5 ppm. There is a spike in Li in the vein with Li concentrations reaching 32.7 ppm. Li concentrations within the amphiboles exhibit a strong sense of homogeneity.

4.3.2 Chlorite

The chlorite Li concentrations show the opposite trend. The higher concentrations are in the block rind, again with higher concentrations in the vein. The block core Li concentrations have a minimum value of 14.8 ppm and the block rind has maximum values of 58.1 ppm. The vein spikes to 62.2 ppm. One thing to note is that there was almost no chlorite in the block rind and this value is based on one grain. Li concentrations within the chlorites exhibit both a homogenous and heterogeneous nature.

4.3.3 Phengite

The phengite Li concentrations also show an increase outwards in the block. The block core has the lower concentrations while the block rind has the higher concentrations. The vein, however, does not spike higher this time but dips to the lowest value. The block core has minimum Li concentrations of 17.4 ppm and the block rind has maximum Li

concentrations of 62.9 ppm. The vein has a low Li concentration of 12.2 ppm. Li concentrations within the phengites also exhibit a strong sense of heterogeneity.

5. Error Analysis

5.1 EPMA

The averages of each composition, the standard deviations, and the relative standard deviations have been calculated for analyses of each mineral from each part of the Mount Hamilton block. The 2σ uncertainties due to counting statistics are calculated by taking the square root of the number of counts collected by the EPMA divided by the number of counts and multiplied by 100. ($2\sigma = 2 \times \frac{\sqrt{n}}{n} \times 100$). To find the uncertainty for minerals that appear heterogeneous, the uncertainty that is given from the EPMA was averaged according to the groupings of the analyses according to different parts of the mineral based on petrographic observations. For example, in one amphibole grain, out of 6 probe spots, 3 are designated as rim and 3 are designated as core. The 3 spots grouped together are averaged and so the uncertainty I acquired from the EPMA on those spots was also be averaged. After this, I used this equation: $\frac{(average\ \ of\ spot \times 2 \times average\ \ of\ uncertainty\ \ )}{100}$.

5.2 LA-ICP-MS

The 2σ uncertainties based on reproducibility and the Poisson's counting statistics have been calculated for all measurements on the laser. The calculation determining the Poisson's statistic used the actual total number of counts (given by the laser). This reproducibility is based on the difference between the ^{6}Li and ^{7}Li results.

The estimated error on the ^{6}Li and ^{7}Li concentration values was calculated by subtracting ^{6}Li from ^{7}Li and dividing by ^{6}Li per analysis. An average deviation of these analyses produced the 2σ values. This was done for each 20 runs of the laser. This represents the reproducibility of the data.

The counting statistic error (Poisson's statistics) was calculated by using this equation: $\frac{1}{\sqrt{.025 \times number\ \ seconds\ \ of\ \ ablation\ \times counts\ \ given\ \ from\ \ laser}}$. Then an average of these analyses was taken. This was done for each the ^{6}Li and ^{7}Li values. Again, this was per 20 analyses. This method is to produce the theoretical potential of uncertainty based on the measurements I took.

The actual observed 2σ of uncertainty produced from the laser is done by multiplying the standard deviation by 2 for each 20 analyses. Something to keep in mind is that the theoretical uncertainty must be less than the observed uncertainty.

5.3 Error Propagation

To propagate EPMA uncertainties the relative variance equation from Potts (1987) was used. The error in the LA-ICP-MS is calculated by summing the relative variances as

follows: Li concentrations = $\sqrt{(\frac{Sa}{a})^2 + \left(\frac{Sb}{b}\right)^2 + (\frac{Sc}{c})^2}$ where $(\frac{Sa}{a})^2$ is the uncertainty from the EPMA, $(\frac{Sb}{b})^2$ is the Poisson counting statistic from the LA-ICP-MS, and $(\frac{Sc}{c})^2$ is the standard deviation of the standard reference material, BCR2g. The 2σ standard deviation of 10 analyses of the silicate glass standard BCR2g is 18.4% and the $2\sigma_{mean}$ is $(\frac{18.4}{\sqrt{10}})$ = 5.8% at 11.6 ppm. The other standard reference material, NIST610, was also calculated for its 2σ standard deviation but not used for error propagation because of the much different Li concentration. The 2σ standard deviation of 57 analyses for NIST610 is 6.8% and the $2\sigma_{mean}$ is $(\frac{6.8}{\sqrt{57}})$ = 0.9% at 493.0 ppm.

6. Discussion of results

6.1 Heterogeneity

One way to asses if these minerals are at equilibrium is by their heterogeneity or homogeneity. To do this, the average Li concentration, standard deviation, and uncertainties are compared. If the standard deviation is greater than the uncertainty then the grain must be heterogeneous. Of all 57 grains analyzed 44 are heterogeneous and the other 13 are homogenous. This implies there is chemical zoning within most of the grains. Out of the 44 heterogeneous grains, 18 are amphiboles, 6 are chlorites, and 20 are phengites. Out of the 13 homogenous grains, 3 are amphiboles, 8 are chlorites, and 2 are phengites.

I predicted that the Li concentrations of the individual minerals would reflect the bulk rock Li concentration, with mineral in the block rind having lower Li concentrations than minerals in the other parts of the block. This prediction held true for the most abundant mineral in the rinds: amphiboles, but not for phengite or chlorite. The measurements of Li concentrations in the phengites are quite heterogeneous, and the ranges of Li concentrations overlap for phengites from all parts of the blocks. The chlorite grain in the rind have a higher Li concentration than chlorite from the other parts of the block, in apparent contradiction to my hypothesis, however since there is only one grain of chlorite, the significance of this difference is not clear.

7. Suggestions for future work

Looking back on this project I see things I could have done differently. This is true in the case of this study. In previous studies, the use of Ba x-ray maps has provided insight into compositional zoning. This could have been useful for this project, although only a small number of the 57 grains I have analyzed would be able to go through this process. This study includes a lot of analyses and the scope of it should not be changed, either to add more analyses or take analyses away.

8. Conclusions

The Mt. Hamilton block, a high-grade block of low-T high-P metamorphic grade out of the Franciscan complex, CA has experienced a complicated history during subduction, and analyzing the different parts of the block can help piece together its subduction history. The relatively unknown processes involving Li exchange during interactions between fluids and rocks in an ancient subduction setting were studied by trace element analysis via LA-ICP-MS of amphiboles, phengites, and chlorites.

The trend is that the Li concentration of the most abundant mineral in the block, amphibole, decreases from block core (11.6 ppm) to block rind (2.2 ppm), mirroring the trend in bulk rock Li concentration. The amphibole Li values were also generally lower than those of the chlorite (22.0 - 46.1 ppm) or phengite (35.9 – 53.8 ppm). The phengites in all parts of the block are heterogeneous, with concentrations in the core ranging from (17.4 – 60.2 ppm) and the rind from (36.8 – 62.9 ppm). Li concentrations of phengites from all parts of the block overlap, so no trend could be discerned between the different parts of the block. The chlorite in the block rind, has higher (35.1 – 58.1 ppm) concentrations of Li than chlorites in the core (14.9 – 25.7 ppm), however the significance of these results in unclear, given that there was only one grain measured in the block rind.

Acknowledgements

I would like to acknowledge my advisors, Sarah Penniston-Dorland, Phil Piccoli, and Bill McDonough, for their hard work in revising, error analysis, machine time, and their time. I would like to thank Richard Ash for his help with the LA-ICP-MS and LAMTRACE. I would like to thank Lin Qiu for his help with editing and suggestions.

Appendix 1: Data Tables:

The following tables include the averaged microprobe analyses of the wt% with the 2σ counting statistics A= amphiboles, C = chlorites, P= phengites.

Table 1: Amphiboles

	Rind																															
	A1		A2			A3			A4 RIM			A4 CORE			A5 RIM			A5 CORE														
# analyses	7			6			7			1			7			3			3												
SiO2	54.80	±0.36	55.79	±0.36	54.41	±0.36	55.12	±0.36	55.57	±0.36	54.40	±0.36	54.53	±0.36																		
TiO2	0.04	±0.02	0.02	±0.41	0.11	±0.03	0.04	±0.02	0.03	±0.02	0.05	±0.05	0.04	±0.02																		
Al2O3	3.99	±0.08	3.03	±0.07	4.40	±0.08	4.91	±0.08	2.62	±0.07	4.90	±0.09	4.41	±0.08																		
FeO	7.32	±0.21	6.85	±0.20	6.02	±0.19	8.26	±0.22	6.99	±0.20	7.35	±0.21	7.24	±0.21																		
MnO	0.16	±0.10	0.23	±0.08	0.20	±0.08	0.16	±0.07	0.21	±0.08	0.14	±0.09	0.19	±0.08																		
MgO	18.30	±0.22	19.03	±0.22	19.69	±0.23	17.22	±0.21	19.15	±0.22	18.07	±0.22	18.16	±0.22																		
CaO	10.80	±0.09	11.22	±0.09	11.30	±0.09	9.58	±0.08	11.55	±0.09	10.72	±0.09	11.16	±0.09																		
Na2O	1.87	±0.06	1.52	±0.05	1.67	±0.06	2.45	±0.07	1.33	±0.05	1.97	±0.06	1.73	±0.06																		
K2O	0.13	±0.01	0.11	±0.01	0.15	±0.01	0.12	±0.01	0.12	±0.01	0.15	±0.02	0.14	±0.01																		
Transition Zone																																
	A1 RIM		A1 CORE		A2 RIM		A2 CORE		A3 RIM		A3 CORE		A4		A5 RIM		A5 RIM 2		A5 CORE												
# analyses	2		2		1		5		5		1		5		2		1		3												
SiO2	57.60	±0.38	47.58	±0.34	57.35	±0.38	47.79	±0.34	53.77	±0.36	46.46	±0.34	57.52	±0.38	54.89	±0.36	57.39	±0.38	46.95	±0.34												
TiO2	0.02	±0.02	0.45	±0.02	0.03	±0.02	0.45	±0.02	0.07	±0.02	0.56	±0.02	0.01	±0.02	0.04	±0.02	0.01	±0.02	0.55	±0.02												
Al2O3	9.69	±0.12	12.42	±0.13	8.90	±0.11	12.11	±0.13	5.48	±0.09	13.31	±0.14	9.24	±0.11	4.51	±0.08	10.09	±0.12	13.02	±0.13												
FeO	13.65	±0.28	12.14	±0.27	13.61	±0.28	11.74	±0.26	11.75	±0.26	11.63	±0.26	14.26	±0.29	11.10	±0.26	13.90	±0.28	11.65	±0.26												
MnO	0.23	±0.08	0.17	±0.07	0.22	±0.09	0.08	±0.10	0.17	±0.08	0.05	±0.08	0.31	±0.09	0.24	±0.08	0.19	±0.08	0.07	±0.08												
MgO	9.69	±0.17	12.73	±0.19	9.98	±0.17	13.20	±0.19	14.96	±0.20	12.82	±0.19	9.38	±0.17	15.70	±0.21	8.77	±0.16	13.03	±0.19												
CaO	1.13	±0.03	9.74	±0.08	2.11	±0.04	9.91	±0.08	9.30	±0.08	9.80	±0.08	1.24	±0.04	9.26	±0.08	0.78	±0.03	9.92	±0.08												
Na2O	6.79	±0.11	3.46	±0.08	6.16	±0.10	3.41	±0.08	2.55	±0.07	3.38	±0.08	6.68	±0.11	2.60	±0.07	7.04	±0.11	3.49	±0.08												
K2O	0.02	±0.01	0.50	±0.02	0.04	±0.01	0.49	±0.02	0.16	±0.01	0.55	±0.02	0.03	±0.01	0.15	±0.01	0.01	±0.01	0.51	±0.02												
Core																																
	A1		A2		A3 RIM		A3 CORE		A4		A5		A6																			
# analyses	6		6		2		4		6		6		5																			
SiO2	46.39	±0.34	46.79	±0.34	52.52	±0.35	46.03	±0.34	46.32	±0.34	46.68	±0.34	45.99	±0.34																		
TiO2	0.59	±0.02	0.52	±0.02	0.14	±0.03	0.57	±0.02	0.57	±0.02	0.52	±0.02	0.60	±0.02																		
Al2O3	13.44	±0.13	13.04	±0.13	5.98	±0.10	13.50	±0.13	12.96	±0.18	12.57	±0.18	13.01	±0.19																		
FeO	11.75	±0.26	11.57	±0.26	11.41	±0.26	12.03	±0.26	11.80	±0.27	11.72	±0.26	11.58	±0.26																		
MnO	0.08	±0.11	0.05	±0.07	0.10	±0.08	0.08	±0.08	0.05	±0.08	0.05	±0.07	0.06	±0.08																		
MgO	12.37	±0.19	12.81	±0.19	15.10	±0.20	12.37	±0.19	12.67	±0.19	12.93	±0.19	12.74	±0.19																		
CaO	9.43	±0.08	9.56	±0.08	10.31	±0.08	9.44	±0.08	9.50	±0.08	9.52	±0.08	9.58	±0.08																		
Na2O	3.66	±0.08	3.58	±0.08	2.33	±0.07	3.63	±0.08	3.78	±0.08	3.68	±0.08	3.69	±0.08																		
K2O	0.61	±0.02	0.60	±0.02	0.24	±0.02	0.60	±0.02	0.60	±0.02	0.58	±0.02	0.58	±0.02																		
Vein																																
	A1 RIM		A1 CORE		A2		A3 RIM		A3 CORE		A4		A5 RIM		A5 CORE																
# analyses	3		3		5		3		3		6		3		3																
SiO2	47.60	±0.34	56.50	±0.37	56.30	±0.36	55.40	±0.37	50.90	±0.35	56.16	±0.34	51.70	±0.35	55.70	±0.37																
TiO2	0.40	±0.03	0.00	±0.01	0.00	±0.02	0.10	±0.08	0.20	±0.03	0.01	±0.02	0.10	±0.02	0.00	±0.02																
Al2O3	10.20	±0.17	10.30	±0.16	9.83	±0.11	10.10	±0.16	7.99	±0.15	8.88	±0.18	7.37	±0.14	9.83	±0.16																
FeO	12.89	±0.28	13.98	±0.29	14.09	±0.28	13.29	±0.28	12.02	±0.27	13.73	±0.27	11.17	±0.26	14.53	±0.29																
MnO	0.13	±0.07	0.22	±0.08	0.25	±0.08	0.18	±0.07	0.12	±0.10	0.29	±0.08	0.09	±0.08	0.26	±0.07																
MgO	12.97	±0.19	8.81	±0.16	9.34	±0.15	10.19	±0.17	14.04	±0.20	8.62	±0.19	15.17	±0.21	8.91	±0.16																
CaO	9.88	±0.08	0.95	±0.03	1.21	±0.04	2.65	±0.08	9.40	±0.08	1.29	±0.08	9.36	±0.08	1.29	±0.04																
Na2O	3.17	±0.08	6.97	±0.11	7.11	±0.11	6.43	±0.11	3.05	±0.08	6.52	±0.08	2.96	±0.08	6.67	±0.11																
K2O	0.43	±0.02	0.02	±0.01	0.03	±0.02	0.09	±0.08	0.36	±0.02	0.02	±0.02	0.28	±0.02	0.03	±0.01																

Table 2: Chlorites

	Rind		Transition Zone																					
	C1		C1		C2		C3		C4		C5a		C5b											
# analyses	10		5		5		5		5		5		1		3									
SiO2	30.96	±0.29	28.84	±0.29	29.08	±0.29	28.81	±0.29	29.42	±0.29	28.58	±0.29	29.03	±0.29										
TiO2	0.005	±0.02	0.00	±0.00	0.00	±0.00	0.00	±0.01	0.00	±0.00	0.00	±0.00	0.00	±0.00										
Al2O3	15.90	±0.21	17.77	±0.22	17.65	±0.22	17.79	±0.22	17.36	±0.22	17.89	±0.22	17.79	±0.22										
Cr2O3	0.00		0.00	±0.00	0.00	±0.00	0.00	±0.00	0.00	±0.00	0.00	±0.00	0.00	±0.00										
FeO	16.71	±0.32	20.47	±0.34	20.99	±0.34	21.49	±0.34	20.87	±0.34	20.97	±0.34	20.93	±0.34										
MnO	0.39	±0.10	0.53	±0.09	0.65	±0.09	0.63	±0.10	0.63	±0.09	0.65	±0.09	0.68	±0.10										
MgO	21.27	±0.26	18.71	±0.26	18.84	±0.26	18.35	±0.26	19.17	±0.26	18.38	±0.26	18.52	±0.26										
CaO	0.14	±0.02	0.04	±0.79	0.03	±0.02	0.00	±0.01	0.01	±0.03	0.05	±0.02	0.03	±0.04										
Na2O	0.02	±0.02	0.02	±0.05	0.04	±0.03	0.02	±0.02	0.02	±0.02	0.21	±0.04	0.04	±0.04										
K2O	0.01	±0.01	0.01	±0.01	0.01	±0.04	0.00	±0.01	0.01	±0.01	0.03	±0.01	0.00	±0.01										
	Core																							
	C1		C2		C4																			
# analyses	4		5		5																			
SiO2	28.76	±0.29	28.77	±0.29	28.44	±0.29																		
TiO2	0.01	±0.02	0.00	±0.05	0.00	±0.00																		
Al2O3	18.00	±0.22	18.32	±0.23	18.00	±0.22																		
Cr2O3	0.00	±0.00	0.00	±0.00	0.00	±0.00																		
FeO	20.47	±0.34	20.74	±0.34	20.86	±0.34																		
MnO	0.67	±0.10	0.60	±0.09	0.65	±0.09																		
MgO	19.00	±0.26	18.95	±0.26	18.57	±0.26																		
CaO	0.01	±0.02	0.00	±0.01	0.01	±0.01																		
Na2O	0.00	±0.03	0.01	±0.02	0.01	±0.01																		
K2O	0.00	±0.07	0.00	±0.01	0.00	±0.02																		
	Vein																							
	C1		C2		C3		C4		C5															
# analyses	5		3		3		1		3															
SiO2	27.55	±0.23	29.11	±0.23	33.97	±0.30	28.05	±0.34	28.94	±0.29														
TiO2	0.03	±0.02	0.00	±0.00	0.00	±0.00	0.00	±0.05	0.01	±0.04														
Al2O3	18.90	±0.37	16.52	±0.37	14.67	±0.20	17.53	±0.22	17.29	±0.23														
Cr2O3	0.00	±0.06	0.00	±0.06	0.00	±0.00	0.00	±0.00	0.00	±0.00														
FeO	23.93	±0.23	22.52	±0.22	14.06	±0.29	20.08	±0.32	21.45	±0.34														
MnO	0.69	±0.27	0.65	±0.27	0.38	±0.07	0.60	±0.13	0.72	±0.12														
MgO	17.82	±0.02	17.80	±0.03	22.73	±0.25	17.53	±0.23	17.99	±0.32														
CaO	0.03	±0.04	0.17	±0.02	0.50	±0.03	0.19	±0.19	0.06	±1.76														
Na2O	0.01	±0.02	0.01	±0.06	0.02	±0.07	0.02	±0.75	0.02	±0.08														
K2O	0.01	±0.10	0.14	±0.09	0.18	±0.02	0.06	±0.18	0.02	±0.02														

Table 3: Phengites

	Rind											
	P1		P2		P3		P4		P5a		P5b	
# analyses		5		5		4		7		2		5
SiO2	50.31	±0.35	49.91	±0.35	51.10	±0.35	50.63	±0.35	50.11	±0.34	51.29	±0.35
TiO2	0.27	±0.02	0.21	±0.02	0.29	±0.02	0.24	±0.02	0.23	±0.02	0.26	±0.02
Al2O3	25.71	±0.24	26.45	±0.25	25.12	±0.24	26.11	±0.24	26.84	±0.25	25.36	±0.24
Cr2O3	0.49	±0.08	0.22	±0.06	0.12	±0.05	0.19	±0.06	0.14	±0.05	0.29	±0.06
FeO	2.44	±0.13	2.15	±0.12	2.54	±0.13	2.34	±0.12	2.25	±0.12	2.33	±0.12
MnO	0.02	±0.09	0.03	±0.12	0.02	±0.09	0.03	±0.07	0.02	±0.06	0.02	±0.05
MgO	4.13	±0.11	3.87	±0.11	4.11	±0.11	3.92	±0.11	3.58	±0.10	4.05	±0.11
CaO	0.01	±0.01	0.02	±0.03	0.03	±0.04	0.00	±0.01	0.00	±0.03	0.02	±0.04
Na2O	0.40	±0.03	0.46	±0.04	0.35	±0.03	0.42	±0.03	0.46	±0.03	0.39	±0.03
K2O	8.11	±0.06	7.88	±0.06	8.03	±0.06	8.30	±0.06	8.50	±0.06	7.84	±0.06
BaO	0.90	±0.06	1.60	±0.07	0.57	±0.06	0.59	±0.06	0.67	±0.06	0.58	±0.06

	Transition Zone															
	P1a		P1b		P2a		P2b		P3		P4		P5a		P5b	
# analyses		4		3		3		4		7		6		1		4
SiO2	50.61	±0.35	49.87	±0.35	50.16	±0.35	50.49	±0.35	49.48	±0.35	50.08	±0.34	42.46	±0.32	49.50	±0.35
TiO2	0.28	±0.02	0.23	±0.02	0.18	±0.02	0.26	±0.02	0.27	±0.02	0.26	±0.02	0.08	±0.02	0.23	±0.02
Al2O3	25.06	±0.24	26.50	±0.25	26.04	±0.25	24.91	±0.24	26.02	±0.25	25.68	±0.24	23.40	±0.24	25.95	±0.24
Cr2O3	0.05	±0.10	0.08	±0.05	0.03	±15.30	0.06	±0.05	0.16	±0.07	0.06	±0.05	0.08	±0.05	0.10	±0.07
FeO	3.10	±0.14	2.66	±0.13	2.95	±0.14	2.93	±0.14	2.70	±0.13	2.79	±0.13	9.75	±0.24	3.01	±0.14
MnO	0.04	±0.08	0.04	±0.06	0.03	±0.30	0.04	±0.06	0.02	±0.06	0.04	±0.10	0.20	±0.07	0.01	±0.03
MgO	4.02	±0.11	3.43	±0.10	3.67	±0.11	4.17	±0.11	3.64	±0.11	3.84	±0.11	8.94	±0.17	3.67	±0.11
CaO	0.00	±0.01	0.00	±0.01	0.00	±0.00	0.00	±0.00	0.00	±0.01	0.00	±0.01	0.02	±0.02	0.00	±0.00
Na2O	0.31	±0.04	0.36	±0.04	0.32	±0.04	0.31	±0.04	0.40	±0.03	0.33	±0.04	0.09	±0.03	0.31	±0.04
K2O	7.77	±0.06	7.90	±0.06	8.31	±0.06	8.02	±0.06	8.58	±0.06	8.44	±0.06	4.64	±0.05	8.35	±0.06
BaO	0.85	±0.06	1.23	±0.06	1.23	±0.06	0.78	±0.06	0.82	±0.06	0.92	±0.06	0.76	±0.05	1.12	±0.06

	Core																			
	P1a		P1b		P1c		P2a		P2b		P3		P4a		P4b		P5a		P5b	
# analyses		2		2		1		2		2		5		2		4		2		4
SiO2	49.93	±0.34	50.88	±0.35	49.09	±0.34	49.21	±0.34	51.85	±0.35	50.08	±0.35	50.83	±0.35	49.51	±0.35	51.33	±0.35	49.72	±0.35
TiO2	0.28	±0.02	0.13	±0.02	0.16	±0.02	0.27	±0.02	0.11	±0.02	0.30	±0.02	0.14	±0.02	0.27	±0.02	0.08	±0.02	0.26	±0.02
Al2O3	25.95	±0.24	24.69	±0.24	27.85	±0.25	26.49	±0.25	23.95	±0.24	25.96	±0.25	23.89	±0.24	25.65	±0.24	24.67	±0.24	26.78	±0.25
Cr2O3	0.02	±0.05	0.06	±0.06	0.05	±0.04	0.11	±0.05	0.06	±0.06	0.05	±0.06	0.04	±0.08	0.07	±0.06	0.07	±0.05	0.06	±0.06
FeO	3.09	±0.14	3.35	±0.14	2.39	±0.12	3.56	±0.15	3.36	±0.15	2.93	±0.14	3.31	±0.14	3.17	±0.14	3.40	±0.15	2.71	±0.13
MnO	0.01	±0.13	0.04	±0.20	0.06	±0.05	0.02	±0.03	0.04	±0.11	0.02	±0.12	0.07	±0.06	0.01	±0.04	0.04	±0.06	0.02	±0.03
MgO	3.84	±0.11	3.98	±0.11	3.19	±0.10	3.63	±0.11	4.28	±0.12	3.68	±0.11	4.06	±0.11	3.73	±0.11	3.98	±0.11	3.53	±0.11
CaO	0.02	±0.02	0.00	±0.00	0.00	±0.00	0.00	±0.00	0.01	±0.02	0.01	±0.02	0.02	±0.02	0.01	±0.03	0.00	±0.00	0.00	±0.00
Na2O	0.40	±0.03	0.12	±0.03	0.44	±0.03	0.43	±0.03	0.09	±0.03	0.41	±0.03	0.11	±0.03	0.39	±0.03	0.14	±0.03	0.39	±0.03
K2O	7.85	±0.06	7.80	±0.06	8.11	±0.06	8.88	±0.06	8.32	±0.06	8.20	±0.06	7.97	±0.06	7.98	±0.06	8.37	±0.06	8.65	±0.06
BaO	0.95	±0.06	1.48	±0.06	1.50	±0.06	0.89	±0.06	1.17	±0.06	0.82	±0.06	1.22	±0.06	0.80	±0.06	0.97	±0.06	1.09	±0.06

	Vein													
	P1a		P1b		P2		P3		P4		P5a		P5b	
# analyses		2		2		2		5		4		2		2
SiO2	50.05	±0.35	50.41	±0.35	50.64	±0.35	50.66	±0.35	51.08	±0.35	52.09	±0.35	51.17	±0.35
TiO2	0.18	±0.02	0.12	±0.02	0.24	±0.02	0.27	±0.02	0.15	±0.16	0.10	±0.02	0.35	±0.02
Al2O3	26.06	±0.24	24.27	±0.24	26.35	±0.25	25.17	±0.24	24.21	±0.25	23.93	±0.23	25.45	±0.24
Cr2O3	0.07	±0.05	0.05	±0.05	0.06	±0.07	0.05	±0.08	0.07	±0.08	0.07	±0.06	0.16	±0.10
FeO	2.66	±0.13	3.36	±0.15	2.95	±0.14	3.16	±0.14	3.65	±0.16	3.32	±0.15	2.97	±0.14
MnO	0.00	±0.00	0.15	±0.07	0.03	±0.04	0.02	±0.12	0.05	±0.19	0.08	±0.10	0.00	±0.00
MgO	3.59	±0.11	4.16	±0.11	3.46	±0.10	3.88	±0.10	4.16	±0.10	4.29	±0.11	3.93	±0.10
CaO	0.00	±0.03	0.02	±0.15	0.00	±0.01	0.01	±0.02	0.00	±0.01	0.02	±0.02	0.02	±0.02
Na2O	0.39	±0.03	0.13	±0.03	0.38	±0.03	0.31	±0.03	0.11	±0.10	0.09	±0.03	0.35	±0.03
K2O	7.95	±0.06	8.11	±0.06	10.12	±0.07	10.46	±0.07	10.46	±0.07	10.41	±0.07	10.10	±0.07
BaO	1.43	±0.06	1.24	±0.06	1.05	±0.05	0.84	±0.05	0.99	±0.29	1.07	±0.05	0.71	±0.04

The following charts include the averaged wt% microprobe analyses plus the 2σ standard deviation of the average. A= Amphiboles, C= Chlorites, P= Phengites

Table 4: Amphiboles

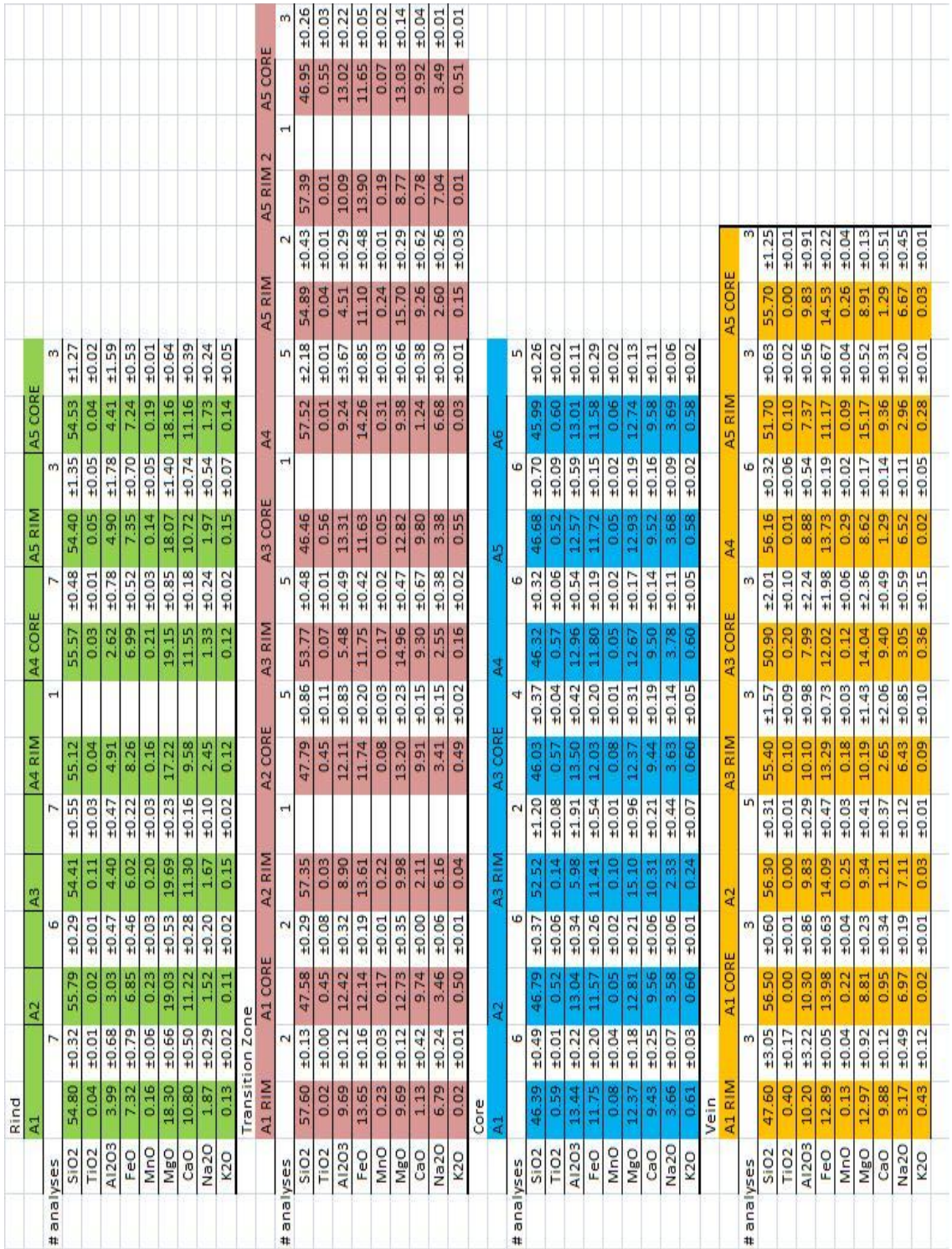

Rind																														
	A1		A2		A3		A4 RIM		A4 CORE		A5 RIM		A5 CORE																	
# analyses	7		6		7		1		7		3		3																	
SiO2	54.80	±0.32	55.79	±0.29	54.41	±0.55	55.12		55.57	±0.48	54.40	±1.35	54.53	±1.27																
TiO2	0.04	±0.01	0.02	±0.01	0.11	±0.03	0.04		0.03	±0.01	0.05	±0.05	0.04	±0.02																
Al2O3	3.99	±0.68	3.03	±0.47	4.40	±0.47	4.91		2.62	±0.78	4.90	±1.78	4.41	±1.59																
FeO	7.32	±0.79	6.85	±0.46	6.02	±0.22	8.26		6.99	±0.52	7.35	±0.70	7.24	±0.53																
MnO	0.16	±0.06	0.23	±0.03	0.20	±0.03	0.16		0.21	±0.03	0.14	±0.05	0.19	±0.01																
MgO	18.30	±0.66	19.03	±0.53	19.69	±0.23	17.22		19.15	±0.85	18.07	±1.40	18.16	±0.64																
CaO	10.80	±0.50	11.22	±0.28	11.30	±0.16	9.58		11.55	±0.18	10.72	±0.74	11.16	±0.39																
Na2O	1.87	±0.29	1.52	±0.20	1.67	±0.10	2.45		1.33	±0.24	1.97	±0.54	1.73	±0.24																
K2O	0.13	±0.02	0.11	±0.02	0.15	±0.02	0.12		0.12	±0.02	0.15	±0.07	0.14	±0.05																
Transition Zone																														
	A1 RIM		A1 CORE		A2 RIM		A2 CORE		A3 RIM		A3 CORE		A4		A5 RIM		A5 RIM 2		A5 CORE											
# analyses	2		2		1		1		5		5		1		2		1		3											
SiO2	57.60	±0.13	47.58	±0.29	57.35		47.79	±0.86	53.77	±0.48	46.46		57.52	±2.18	54.89	±0.43	57.39		46.95	±0.26										
TiO2	0.02	±0.00	0.45	±0.08	0.03		0.45	±0.11	0.07	±0.01	0.56		0.01	±0.01	0.04	±0.01	0.01		0.55	±0.03										
Al2O3	9.69	±0.12	12.42	±0.32	8.90		12.11	±0.83	5.48	±0.49	13.31		9.24	±3.67	4.51	±0.29	10.09		13.02	±0.22										
FeO	13.65	±0.16	12.14	±0.19	13.61		11.74	±0.20	11.75	±0.42	11.63		14.26	±0.85	11.10	±0.48	13.90		11.65	±0.05										
MnO	0.23	±0.03	0.17	±0.01	0.22		0.08	±0.03	0.17	±0.02	0.05		0.31	±0.03	0.24	±0.01	0.19		0.07	±0.02										
MgO	9.69	±0.12	12.73	±0.35	9.98		13.20	±0.23	14.96	±0.47	12.82		9.38	±0.66	15.70	±0.29	8.77		13.03	±0.14										
CaO	1.13	±0.42	9.74	±0.00	2.11		9.91	±0.15	9.30	±0.67	9.80		1.24	±0.38	9.26	±0.62	0.78		9.92	±0.04										
Na2O	6.79	±0.24	3.46	±0.06	6.16		3.41	±0.15	2.55	±0.38	3.38		6.68	±0.30	2.60	±0.26	7.04		3.49	±0.01										
K2O	0.02	±0.01	0.50	±0.01	0.04		0.49	±0.02	0.16	±0.02	0.55		0.03	±0.01	0.15	±0.03	0.01		0.51	±0.01										
Core																														
	A1		A2		A3 RIM		A3 CORE		A4		A5		A6																	
# analyses	6		6		2		4		6		6		5																	
SiO2	46.39	±0.49	46.79	±0.37	52.52	±1.20	46.03	±0.37	46.32	±0.32	46.68	±0.70	45.99	±0.26																
TiO2	0.59	±0.01	0.52	±0.06	0.14	±0.08	0.57	±0.04	0.57	±0.06	0.52	±0.09	0.60	±0.02																
Al2O3	13.44	±0.22	13.04	±0.34	5.98	±1.91	13.50	±0.42	12.96	±0.54	12.57	±0.59	13.01	±0.11																
FeO	11.75	±0.20	11.57	±0.26	11.41	±0.54	12.03	±0.20	11.80	±0.19	11.72	±0.15	11.58	±0.29																
MnO	0.08	±0.04	0.05	±0.02	0.10	±0.01	0.08	±0.01	0.05	±0.02	0.05	±0.02	0.06	±0.02																
MgO	12.37	±0.18	12.81	±0.21	15.10	±0.96	12.37	±0.31	12.67	±0.17	12.93	±0.19	12.74	±0.13																
CaO	9.43	±0.25	9.56	±0.06	10.31	±0.21	9.44	±0.19	9.50	±0.14	9.52	±0.16	9.58	±0.11																
Na2O	3.66	±0.07	3.58	±0.06	2.33	±0.44	3.63	±0.14	3.78	±0.11	3.68	±0.09	3.69	±0.06																
K2O	0.61	±0.03	0.60	±0.01	0.24	±0.07	0.60	±0.05	0.60	±0.05	0.58	±0.02	0.58	±0.02																
Vein																														
	A1 RIM		A1 CORE		A2		A3 RIM		A3 CORE		A4		A5 RIM		A5 CORE															
# analyses	3		3		5		3		3		3		3		3															
SiO2	47.60	±3.05	56.50	±0.60	56.30	±0.31	55.40	±1.57	50.90	±2.01	56.16	±0.32	51.70	±0.63	55.70	±1.25														
TiO2	0.40	±0.17	0.00	±0.01	0.00	±0.01	0.10	±0.09	0.20	±0.10	0.01	±0.06	0.10	±0.02	0.00	±0.01														
Al2O3	10.20	±3.22	10.30	±0.86	9.83	±0.29	10.10	±0.98	7.99	±2.24	8.88	±0.54	7.37	±0.56	9.83	±0.91														
FeO	12.89	±0.05	13.98	±0.63	14.09	±0.47	13.29	±0.73	12.02	±1.98	13.73	±0.19	11.17	±0.67	14.53	±0.22														
MnO	0.13	±0.04	0.22	±0.04	0.25	±0.03	0.18	±0.03	0.12	±0.06	0.29	±0.02	0.09	±0.04	0.26	±0.04														
MgO	12.97	±0.92	8.81	±0.23	9.34	±0.41	10.19	±1.43	14.04	±2.36	8.62	±0.17	15.17	±0.52	8.91	±0.13														
CaO	9.88	±0.12	0.95	±0.34	1.21	±0.37	2.65	±2.06	9.40	±0.49	1.29	±0.14	9.36	±0.31	1.29	±0.51														
Na2O	3.17	±0.49	6.97	±0.19	7.11	±0.12	6.43	±0.85	3.05	±0.59	6.52	±0.11	2.96	±0.20	6.67	±0.45														
K2O	0.43	±0.12	0.02	±0.01	0.03	±0.01	0.09	±0.10	0.36	±0.15	0.02	±0.05	0.28	±0.01	0.03	±0.01														

Table 5: Chlorites

	Rind		Transition Zone											
	C1		C1		C2		C3		C4		C5a		C5b	
# analyses		10		5		5		5		5		1		3
SiO2	30.96	±0.01	28.84	±0.15	29.08	±0.16	28.81	±0.27	29.42	±0.28	28.58		29.03	±0.40
TiO2	0.00	±3.80	0.00	±0.00	0.00	±0.00	0.00	±0.00	0.00	±0.00	0.00		0.00	±0.00
Al2O3	15.90	±0.01	17.77	±0.16	17.65	±0.13	17.79	±0.20	17.36	±0.13	17.89		17.79	±0.31
Cr2O3	0.00		0.00	±0.00	0.00	±0.00	0.00	±0.00	0.00	±0.00	0.00		0.00	±0.00
FeO	16.71	±0.01	20.47	±0.32	20.99	±0.51	21.49	±0.21	20.87	±0.39	20.97		20.93	±0.44
MnO	0.39	±0.32	0.53	±0.03	0.65	±0.03	0.63	±0.04	0.63	±0.04	0.65		0.68	±0.02
MgO	21.27	±0.01	18.71	±0.23	18.84	±0.30	18.35	±0.12	19.17	±0.47	18.38		18.52	±0.31
CaO	0.14	±4.47	0.04	±0.05	0.03	±0.01	0.00	±0.00	0.01	±0.01	0.05		0.03	±0.02
Na2O	0.02	±24.49	0.02	±0.02	0.04	±0.01	0.02	±0.01	0.02	±0.01	0.21		0.04	±0.08
K2O	0.01	±65.07	0.01	±0.01	0.01	±0.00	0.00	±0.00	0.01	±0.01	0.03		0.00	±0.01

	Core					
	C1		C2		C4	
# analyses		4		5		5
SiO2	28.76	±0.12	28.77	±0.32	28.44	±0.44
TiO2	0.01	±0.02	0.00	±0.01	0.00	±0.00
Al2O3	18.00	±0.20	18.32	±0.43	18.00	±0.34
Cr2O3	0.00	±0.00	0.00	±0.00	0.00	±0.00
FeO	20.47	±0.30	20.74	±0.21	20.86	±0.24
MnO	0.67	±0.05	0.60	±0.08	0.65	±0.03
MgO	19.00	±0.18	18.95	±0.24	18.57	±0.34
CaO	0.01	±0.01	0.00	±0.01	0.01	±0.01
Na2O	0.00	±0.00	0.01	±0.01	0.01	±0.01
K2O	0.00	±0.00	0.00	±0.00	0.00	±0.00

	Vein									
	C1		C2		C3		C4		C5	
# analyses		5		3		3		1		3
SiO2	27.55	±0.16	29.11	±0.99	33.97	±1.36	28.05		28.94	±0.28
TiO2	0.03	±0.01	0.00	±0.00	0.00	±0.00	0.00		0.01	±0.02
Al2O3	18.90	±0.26	16.52	±1.03	14.67	±0.80	17.53		17.29	±0.42
Cr2O3	0.00	±0.00	0.00	±0.00	0.00	±0.00	0.00		0.00	±0.00
FeO	23.93	±0.16	22.52	±2.04	14.06	±0.31	20.08		21.45	±0.30
MnO	0.69	±0.03	0.65	±0.06	0.38	±0.04	0.60		0.72	±0.07
MgO	17.82	±0.27	17.80	±0.34	22.73	±0.15	17.53		17.99	±0.46
CaO	0.03	±0.01	0.17	±0.09	0.50	±0.08	0.19		0.06	±0.04
Na2O	0.01	±0.01	0.01	±0.00	0.02	±0.01	0.02		0.02	±0.01
K2O	0.01	±0.01	0.14	±0.12	0.18	±0.06	0.06		0.02	±0.01

Table 6: Phengites

	Rind											
	Sampl	P1		P2		P3		P4		P5a		P5b	
# analyses			5		5		4		7		2		5
	SiO2	50.31	±0.54	49.91	±0.42	51.10	±0.40	50.63	±0.58	50.11	±0.23	51.29	±0.27
	TiO2	0.27	±0.02	0.21	±0.02	0.29	±0.01	0.24	±0.03	0.23	±0.01	0.26	±0.01
	Al2O3	25.71	±0.60	26.45	±0.19	25.12	±0.36	26.11	±0.59	26.84	±0.02	25.36	±0.67
	Cr2O3	0.49	±0.15	0.22	±0.04	0.12	±0.01	0.19	±0.04	0.14	±0.01	0.29	±0.03
	FeO	2.44	±0.25	2.15	±0.06	2.54	±0.19	2.34	±0.17	2.25	±0.03	2.33	±0.18
	MnO	0.02	±0.02	0.03	±0.02	0.02	±0.02	0.03	±0.02	0.02	±0.01	0.02	±0.01
	MgO	4.13	±0.24	3.87	±0.12	4.11	±0.06	3.92	±0.18	3.58	±0.15	4.05	±0.04
	CaO	0.01	±0.01	0.02	±0.02	0.03	±0.02	0.00	±0.00	0.00	±0.00	0.02	±0.02
	Na2O	0.40	±0.04	0.46	±0.01	0.35	±0.02	0.42	±0.02	0.46	±0.00	0.39	±0.01
	K2O	8.11	±0.57	7.88	±0.24	8.03	±0.12	8.30	±0.24	8.50	±0.40	7.84	±0.25
	BaO	0.90	±0.32	1.60	±0.10	0.57	±0.04	0.59	±0.11	0.67	±0.07	0.58	±0.07

	Transition Zone																	
	Sampl	P1a		P1b		P2a		P2b		P3		P4		P5a		P5b		
# analyses			4		3		3		4		7		6		1		4	
	SiO2	50.61	±0.31	49.87	±0.42	50.16	±0.77	50.49	±1.04	49.48	±0.54	50.08	±0.68	42.46		49.50	±0.24	
	TiO2	0.28	±0.04	0.23	±0.03	0.18	±0.03	0.26	±0.09	0.27	±0.01	0.26	±0.05	0.08		0.23	±0.10	
	Al2O3	25.06	±0.82	26.50	±0.79	26.04	±1.05	24.91	±1.47	26.02	±0.18	25.68	±0.90	23.40		25.95	±1.11	
	Cr2O3	0.05	±0.03	0.08	±0.02	0.03	±0.03	0.06	±0.02	0.16	±0.08	0.06	±0.03	0.08		0.10	±0.05	
	FeO	3.10	±0.30	2.66	±0.22	2.95	±0.40	2.93	±0.24	2.70	±0.07	2.79	±0.17	9.75		3.01	±0.53	
	MnO	0.04	±0.02	0.04	±0.01	0.03	±0.02	0.04	±0.01	0.02	±0.01	0.04	±0.02	0.20		0.01	±0.01	
	MgO	4.02	±0.26	3.43	±0.23	3.67	±0.38	4.17	±0.61	3.64	±0.14	3.84	±0.28	8.94		3.67	±0.36	
	CaO	0.00	±0.01	0.00	±0.00	0.00	±0.00	0.00	±0.00	0.00	±0.00	0.00	±0.01	0.02		0.00	±0.00	
	Na2O	0.31	±0.10	0.36	±0.10	0.32	±0.12	0.31	±0.12	0.40	±0.02	0.33	±0.08	0.09		0.31	±0.16	
	K2O	7.77	±0.08	7.90	±0.20	8.31	±0.36	8.02	±0.15	8.58	±0.42	8.44	±0.18	4.64		8.35	±0.18	
	BaO	0.85	±0.08	1.23	±0.09	1.23	±0.10	0.78	±0.09	0.82	±0.17	0.92	±0.12	0.76		1.12	±0.10	

	Core																					
		P1a		P1b		P1c		P2a		P2b		P3		P4a		P4b		P5a		P5b		
# analyses			2		2		1		2		2		5		2		4		2		4	
	SiO2	49.93	±0.19	50.88	±0.12	49.09		49.21	±0.09	51.85	±0.50	50.08	±0.34	50.83	±0.21	49.51	±0.39	51.33	±0.39	49.72	±0.26	
	TiO2	0.28	±0.02	0.13	±0.07	0.16		0.27	±0.01	0.11	±0.03	0.30	±0.02	0.14	±0.02	0.27	±0.01	0.08	±0.01	0.26	±0.03	
	Al2O3	25.95	±0.08	24.69	±0.53	27.85		26.49	±0.08	23.95	±0.39	25.96	±0.20	23.89	±0.95	25.65	±0.29	24.67	±0.32	26.78	±0.27	
	Cr2O3	0.02	±0.01	0.06	±0.02	0.05		0.11	±0.00	0.06	±0.03	0.05	±0.02	0.04	±0.03	0.07	±0.03	0.07	±0.01	0.06	±0.02	
	FeO	3.09	±0.26	3.35	±0.15	2.39		3.56	±0.00	3.36	±0.23	2.93	±0.21	3.31	±0.02	3.17	±0.37	3.40	±0.23	2.71	±0.04	
	MnO	0.01	±0.01	0.04	±0.03	0.06		0.02	±0.02	0.04	±0.03	0.02	±0.01	0.07	±0.01	0.01	±0.01	0.04	±0.02	0.02	±0.02	
	MgO	3.84	±0.00	3.98	±0.23	3.19		3.63	±0.02	4.28	±0.34	3.68	±0.04	4.06	±0.13	3.73	±0.06	3.98	±0.05	3.53	±0.08	
	CaO	0.02	±0.00	0.00	±0.00	0.00		0.00	±0.00	0.01	±0.01	0.01	±0.01	0.02	±0.00	0.01	±0.00	0.00	±0.00	0.00	±0.00	
	Na2O	0.40	±0.02	0.12	±0.02	0.44		0.43	±0.01	0.09	±0.00	0.41	±0.01	0.11	±0.04	0.39	±0.03	0.14	±0.02	0.39	±0.00	
	K2O	7.85	±0.02	7.80	±0.08	8.11		8.88	±0.00	8.32	±0.15	8.20	±0.06	7.97	±0.24	7.98	±0.13	8.37	±0.02	8.65	±0.23	
	BaO	0.95	±0.06	1.48	±0.12	1.50		0.89	±0.10	1.17	±0.09	0.82	±0.11	1.22	±0.15	0.80	±0.14	0.97	±0.05	1.09	±0.07	

	Vein														
		P1a		P1b		P2		P3		P4		P5a		P5b	
# analyses			2		2		2		5		4		2		2
	SiO2	50.05	±0.04	50.41	±0.13	50.64	±0.45	50.66	±0.43	51.08	±0.33	52.09	±0.29	51.17	±0.42
	TiO2	0.18	±0.04	0.12	±0.00	0.24	±0.02	0.27	±0.06	0.15	±0.01	0.10	±0.01	0.35	±0.02
	Al2O3	26.06	±0.21	24.27	±0.15	26.35	±0.21	25.17	±0.10	24.21	±0.24	23.93	±0.42	25.45	±0.00
	Cr2O3	0.07	±0.02	0.05	±0.00	0.06	±0.02	0.05	±0.03	0.07	±0.01	0.07	±0.01	0.16	±0.09
	FeO	2.66	±0.14	3.36	±0.06	2.95	±0.02	3.16	±0.19	3.65	±0.23	3.32	±0.19	2.97	±0.17
	MnO	0.00	±0.00	0.15	±0.06	0.03	±0.03	0.02	±0.02	0.05	±0.03	0.08	±0.05	0.00	±0.00
	MgO	3.59	±0.22	4.16	±0.31	3.46	±0.01	3.88	±0.07	4.16	±0.06	4.29	±0.12	3.93	±0.04
	CaO	0.00	±0.00	0.02	±0.02	0.00	±0.00	0.01	±0.01	0.00	±0.00	0.02	±0.00	0.02	±0.00
	Na2O	0.39	±0.05	0.13	±0.00	0.38	±0.01	0.31	±0.05	0.11	±0.01	0.09	±0.00	0.35	±0.02
	K2O	7.95	±0.34	8.11	±0.24	10.12	±0.03	10.46	±0.06	10.46	±0.07	10.41	±0.05	10.10	±0.03
	BaO	1.43	±0.20	1.24	±0.12	1.05	±0.10	0.84	±0.09	0.99	±0.08	1.07	±0.03	0.71	±0.01

Table 7: Amphibole classification by location in both the block and grain (rim v core)

Sample	Name
A1	Actinolite
A2	Actinolite
A3	Tremolite
A4 RIM	Winchite
A4 CORE	Actinolite
A5 RIM	Actinolite
A5 CORE	Actinolite
A1 RIM	Glaucophane
A1 CORE	Magnesiokatophorite
A2 RIM	Glaucophane
A2 CORE	Edenite
A3 RIM	Winchite
A3 CORE	Magnesiokatophorite
A4	Glaucophane
A5 RIM	Winchite
A5 RIM 2	Glaucophane
A5 CORE	Edenite

Sample	Name
A1	Magnesiokatophorite
A2	Magnesiokatophorite
A3 RIM	Magnesiohornblende
A3 CORE	Magnesiokatophorite
A4	Magnesiokatophorite
A5	Magnesiokatophorite
A6	Magnesiokatophorite
A1 RIM	Magnesiohornblende
A1 CORE	Glaucophane
A2	Glaucophane
A3 RIM	Glaucophane
A3 CORE	Barroisite
A4	Glaucophane
A5 RIM	Barroisite
A5 CORE	Glaucophane

Table 7: Average Li concentrations per part and mineral of the Mt. Hamilton block. Included are the ±2σ propagated standard deviations as well as the range of Li concentrations (all values in ppm)

	Amphibole	Range	**Chlorite**	Range	**Phengite**	Range
Rind	2.2 ±0.2	0.5-11.4	46.1 ±5.3	35.1-58.1	53.8 ±3.3	36.8-62.9
Transition	11.9 ±0.7	1.9-28.3	24.3 ±1.5	21.9-28.9	40.1 ±2.5	25.8-57.5
Core	11.6 ±0.8	4.1-28.0	22.0 ±1.4	14.9-25.7	40.6 ±2.5	17.4-60.2
Vein	14.8 ±1.1	4.1-32.7	37.1 ±2.7	19.2-62.4	35.9 ±2.2	12.2-51.6

Appendix 2: Grains

The following are the study grains, all are labeled with Li concentrations (in ppm), scales, and 2σ errors. The grains are grouped by the part of the block in which they occur.

Block Rind

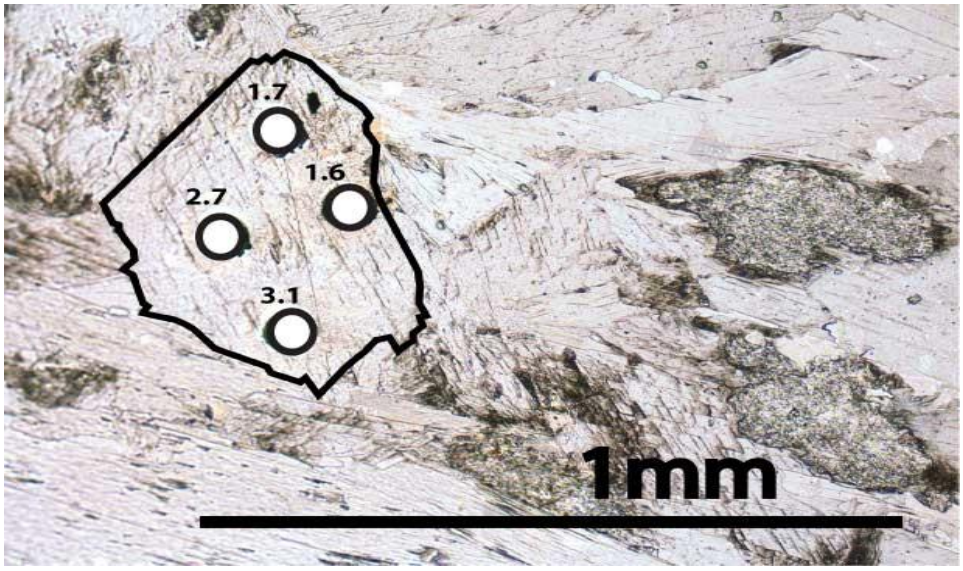

Figure 8: GL16-4 Amphibole 1 10x all Li concentrations ±0.2

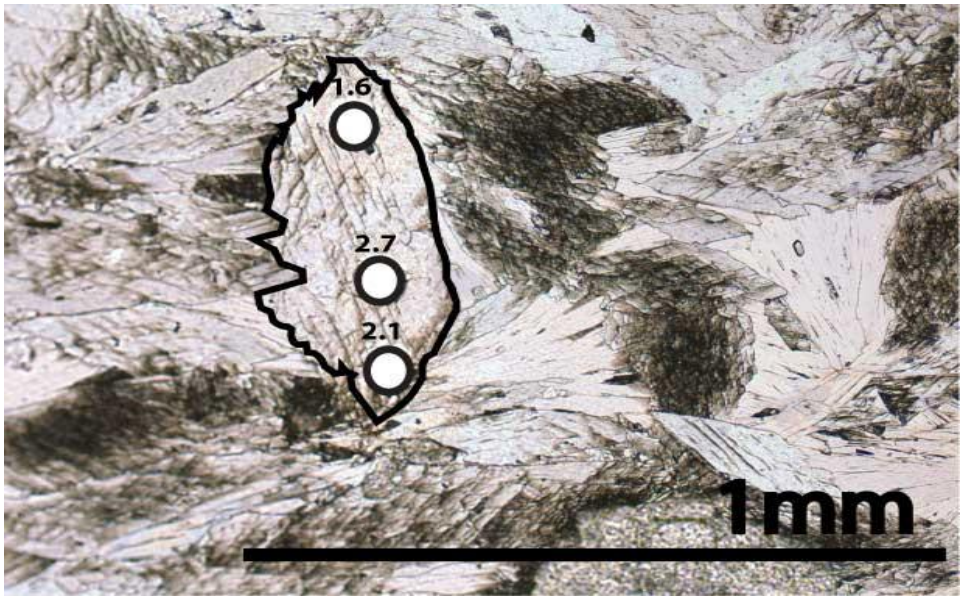

Figure 9: GL 16-4 Amphibole 2 10x all Li concentrations ±0.2

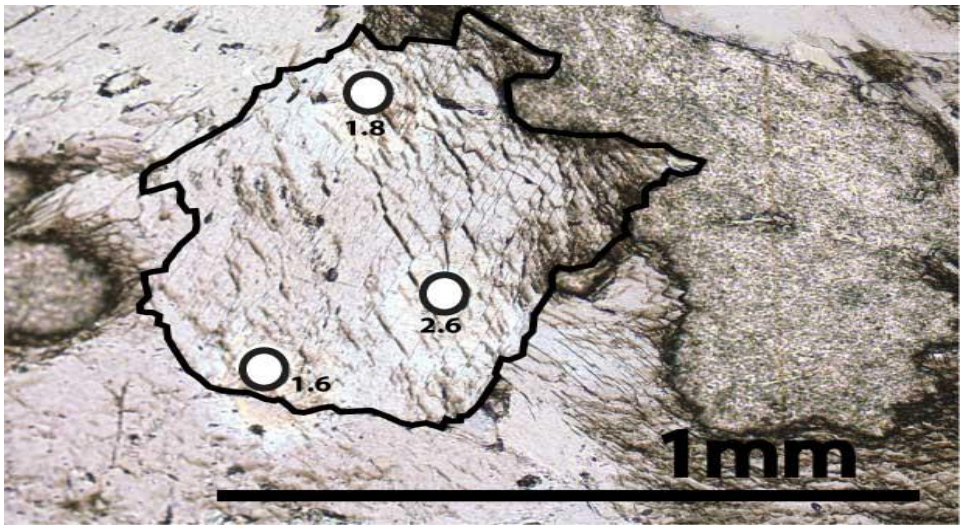

Figure 10: GL 16-4 Amphibole 3 10x all Li concentrations ±0.2

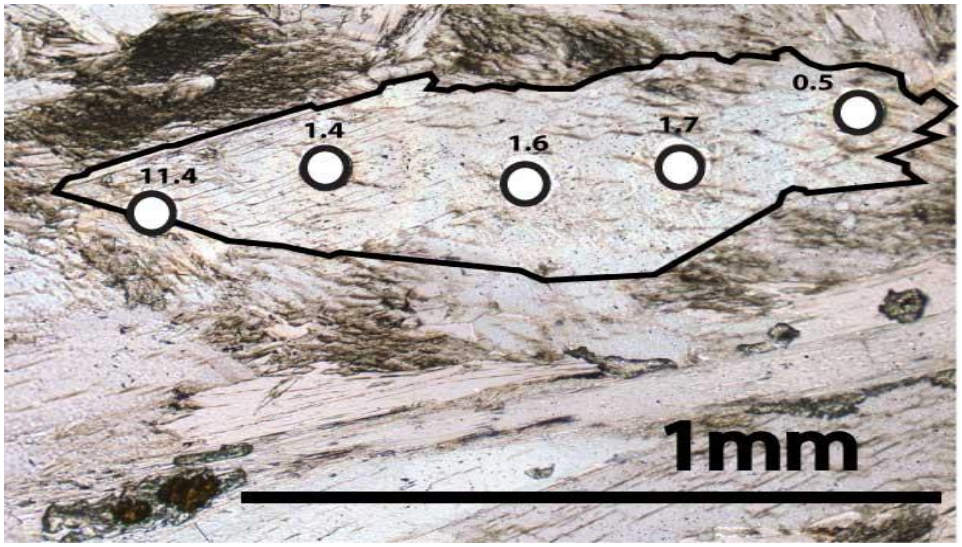

Figure 11: GL16-4 Amphibole 4 10x all Li concentrations ±0.2

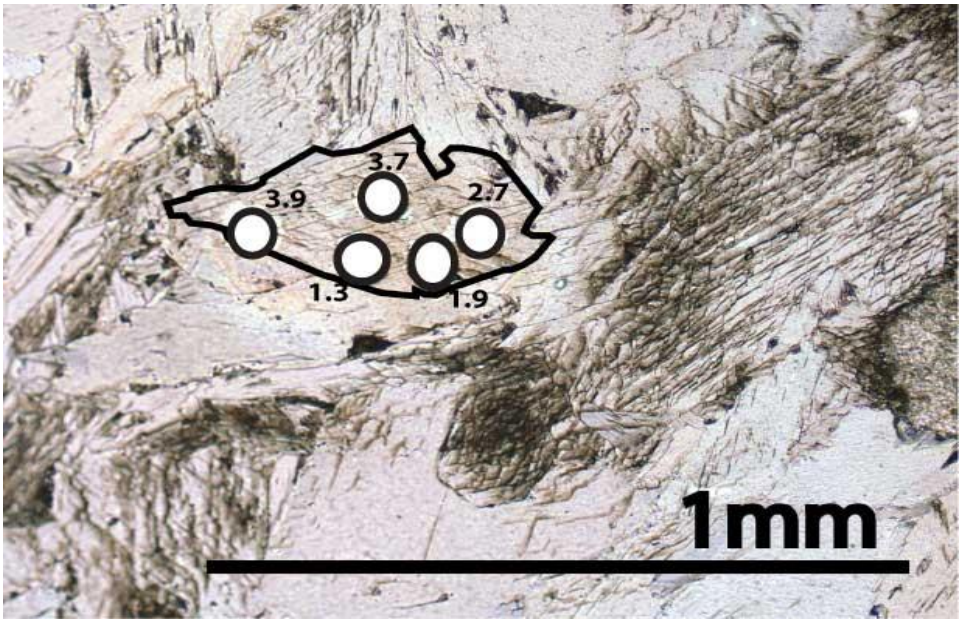

Figure 12: GL16-4 Amphibole 5 10x all Li concentrations ±0.2

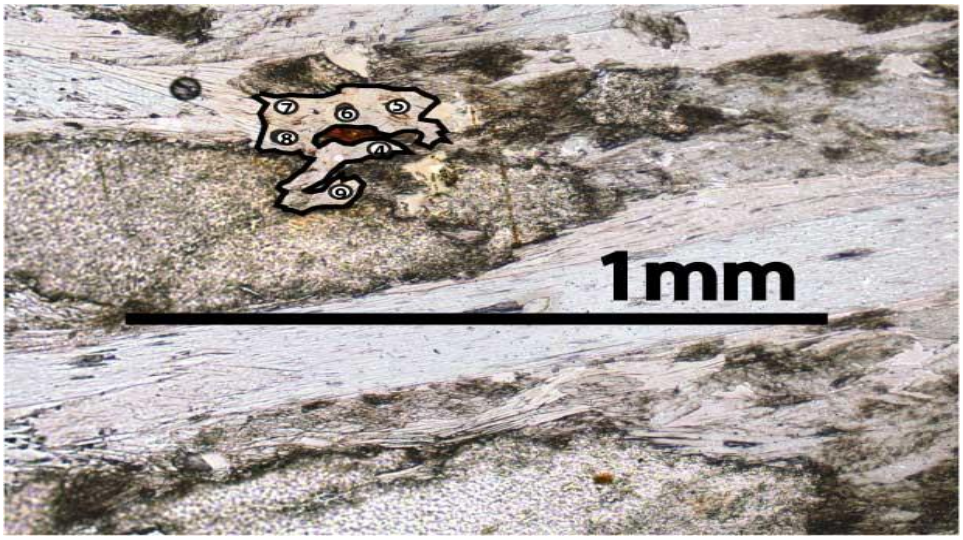

Figure 13: GL16-4 Chlorite 1 10x all Li concentrations ±5.3

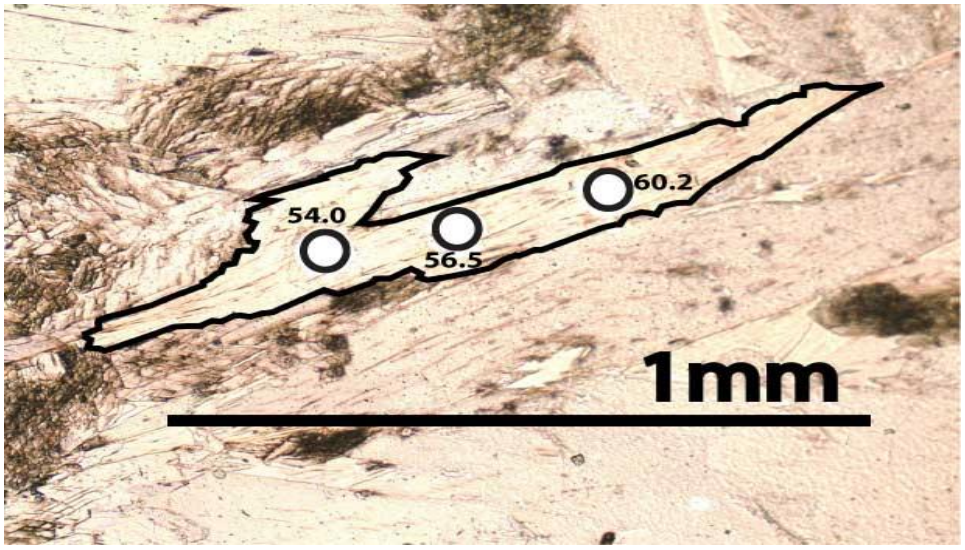

Figure 14: GL16-4 Phengite 1 10x all Li concentrations ±3.3

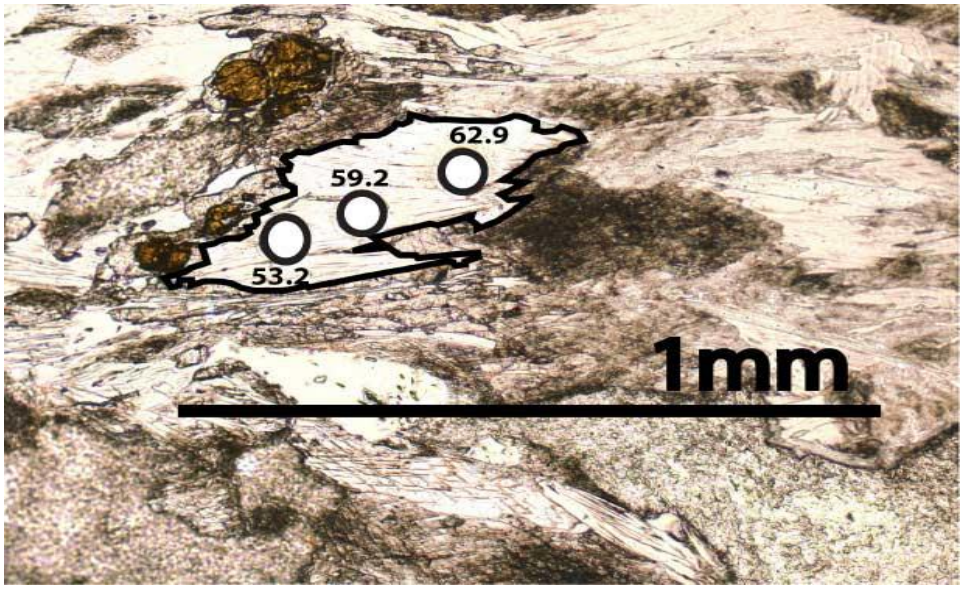

Figure 15: GL16-4 Phengite 2 10x all Li concentrations ±3.3

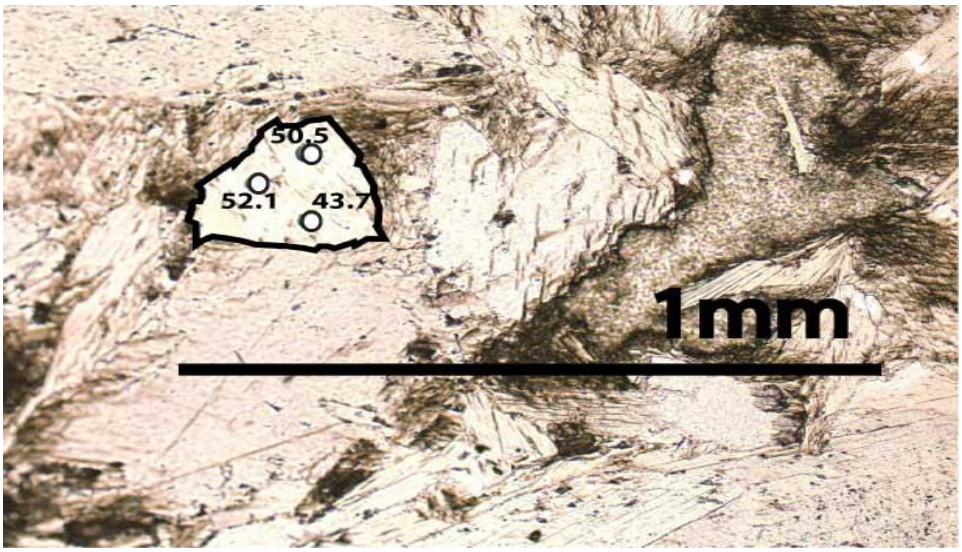

Figure 16: GL16-4 Phengite 3 10x all Li concentrations ±3.3

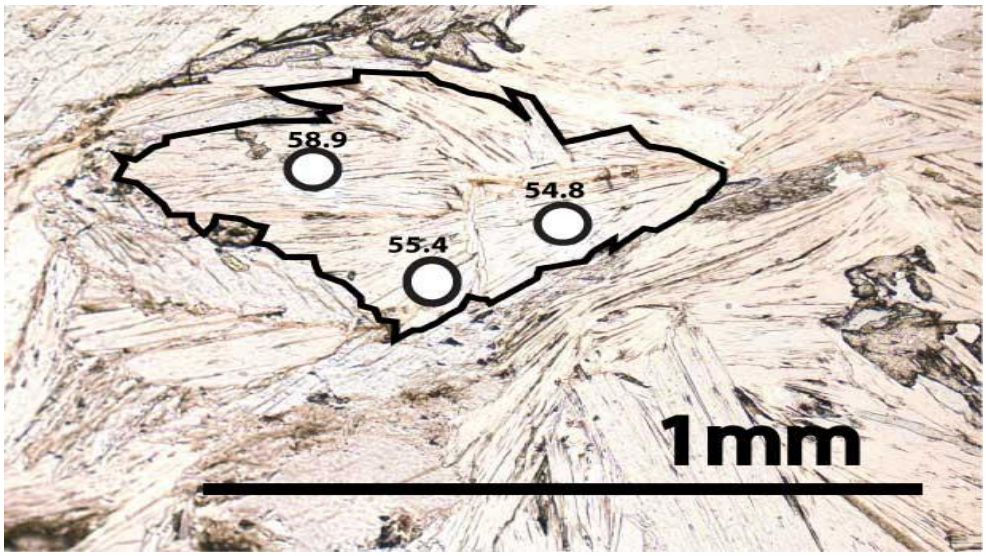

Figure 17: GL16-4 Phengite 4 10x all Li concentrations ±3.3

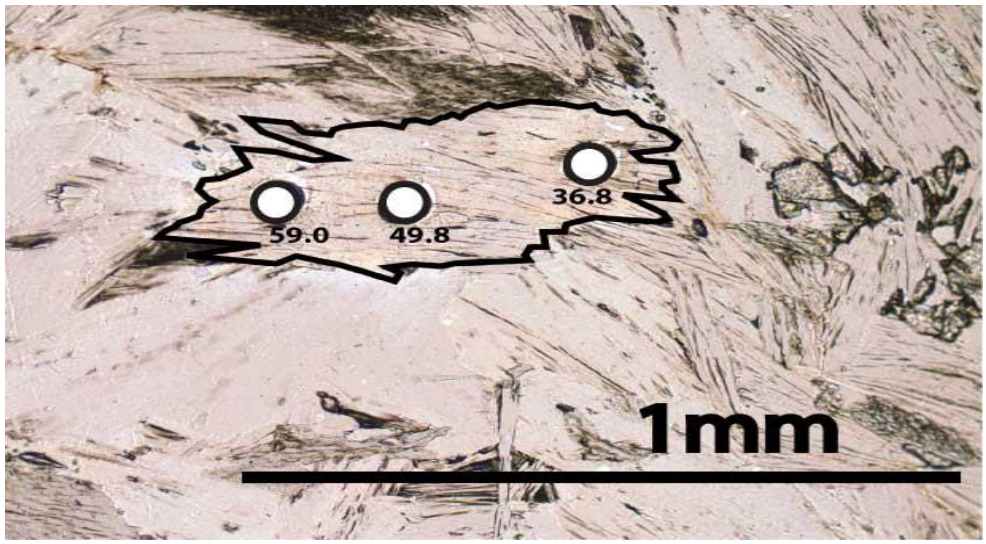

Figure 18: GL16-4 Phengite 5 10x all Li concentrations ±3.3

Transition Zone

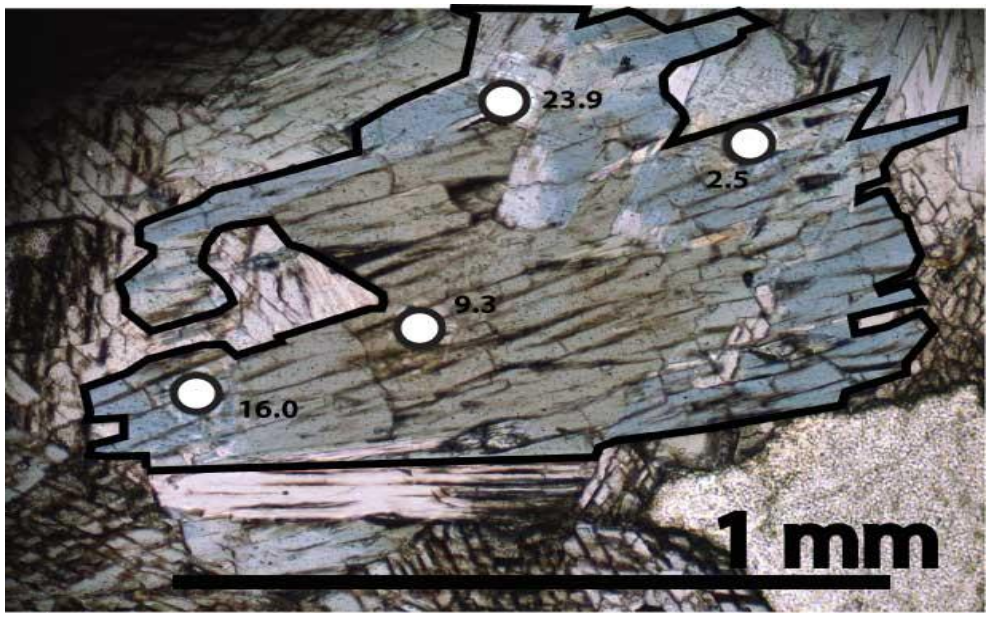

Figure 19: MH90-9 Amphibole 1 10x all Li concentrations ±0.7

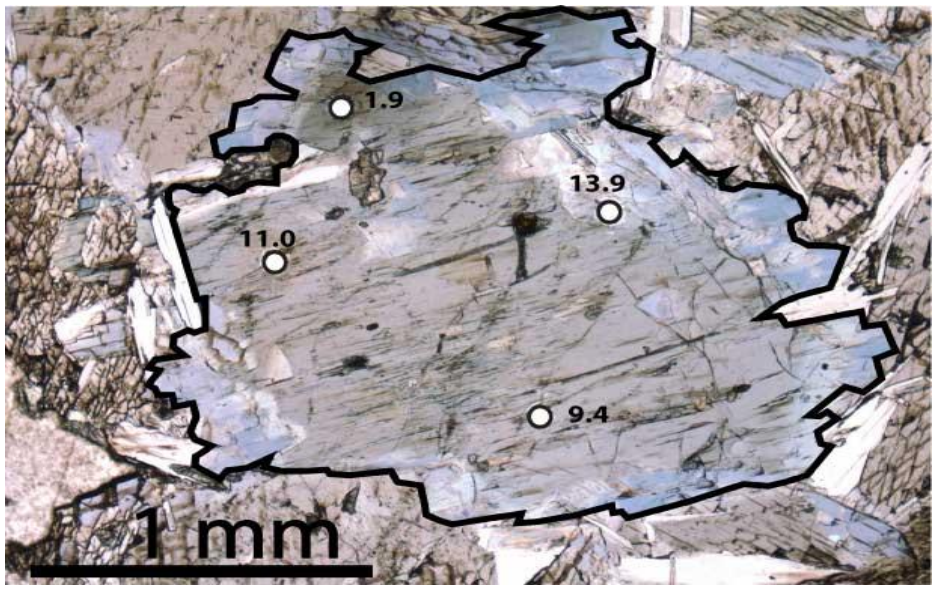

Figure 20: MH90-9 Amphibole 2 5x all Li concentrations ±0.7

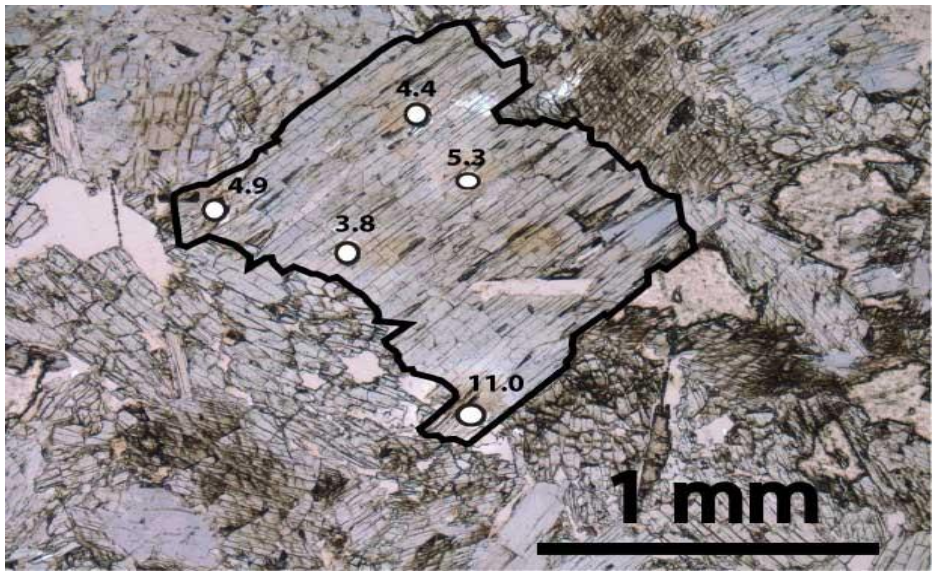

Figure 21: MH90-9 Amphibole 3 5x all Li concentrations ±0.7

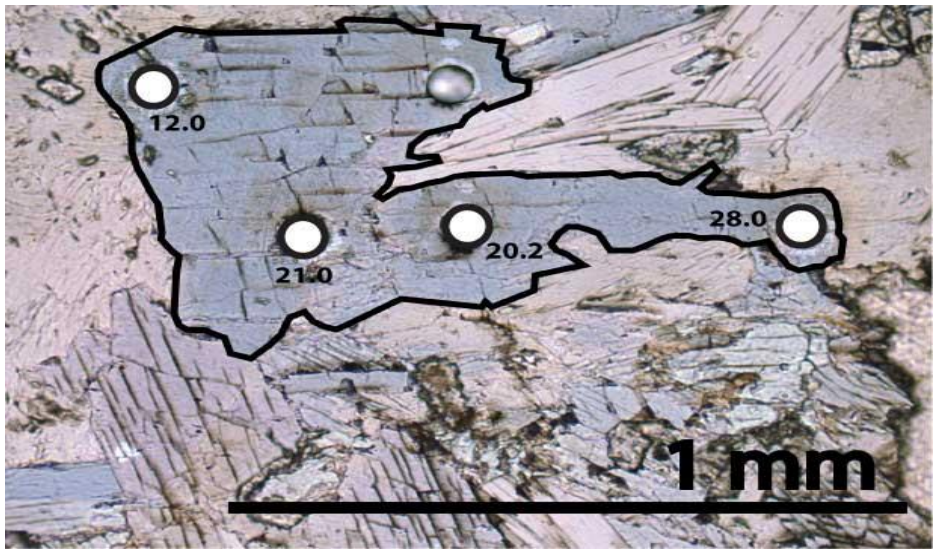

Figure 22: MH90-9 Amphibole 4 10x all Li concentrations ±0.7

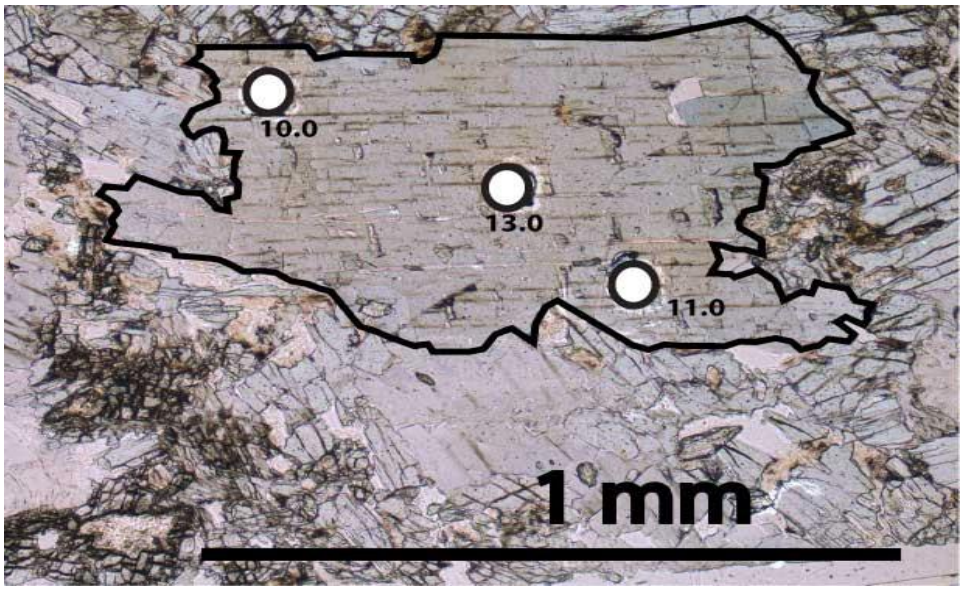

Figure 23: MH90-9 Amphibole 5 10x all Li concentrations ±0.7

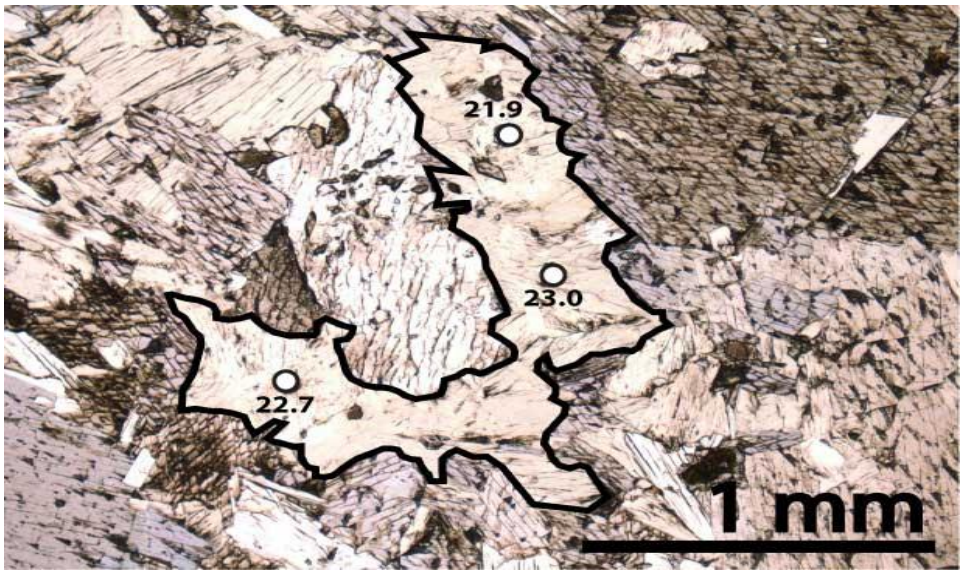

Figure 24: MH90-9 Chlorite 1 5x all Li concentrations ±1.5

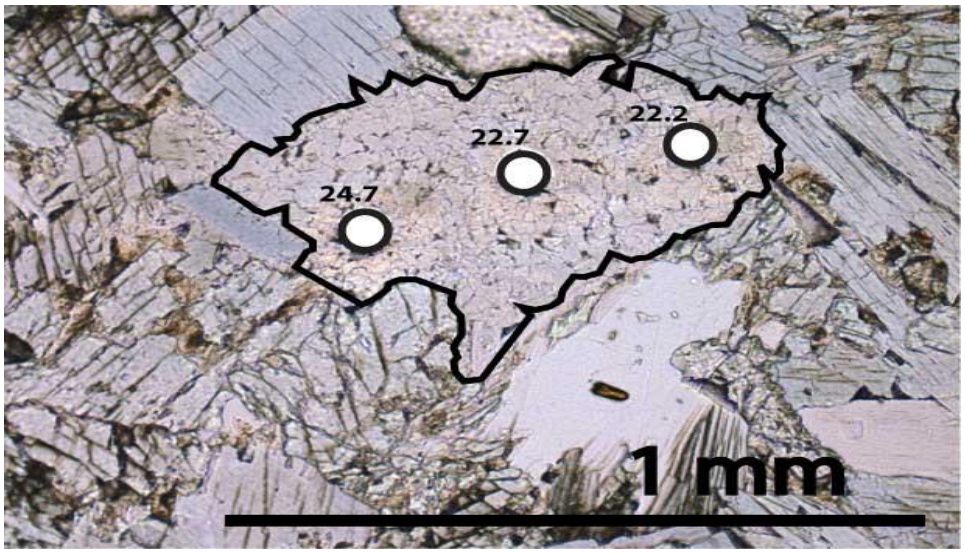

Figure 25: MH90-9 Chlorite 2 10x all Li concentrations ±1.5

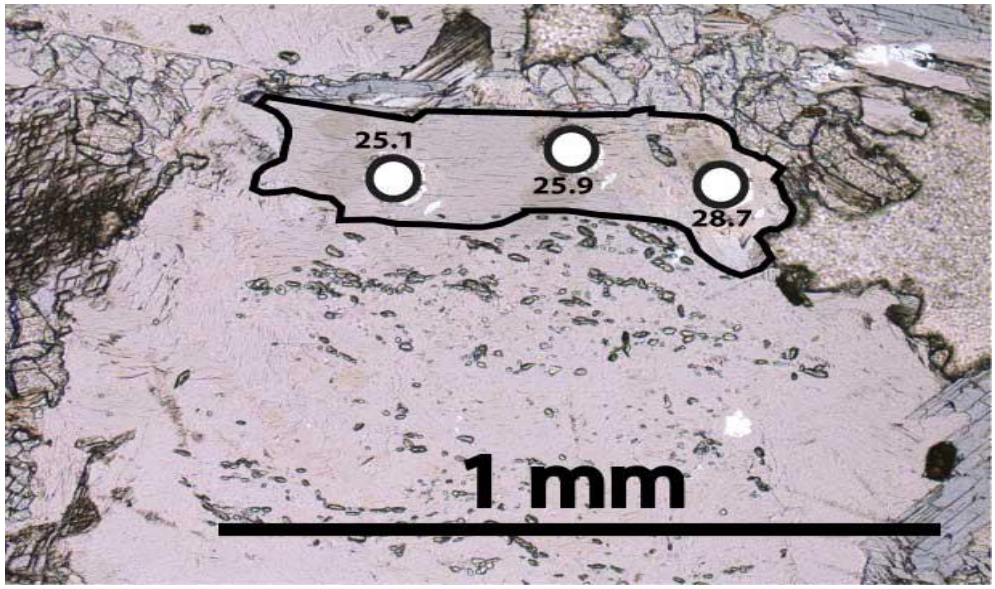

Figure 26: MH90-9 Chlorite 3 10x all Li concentrations ±1.5

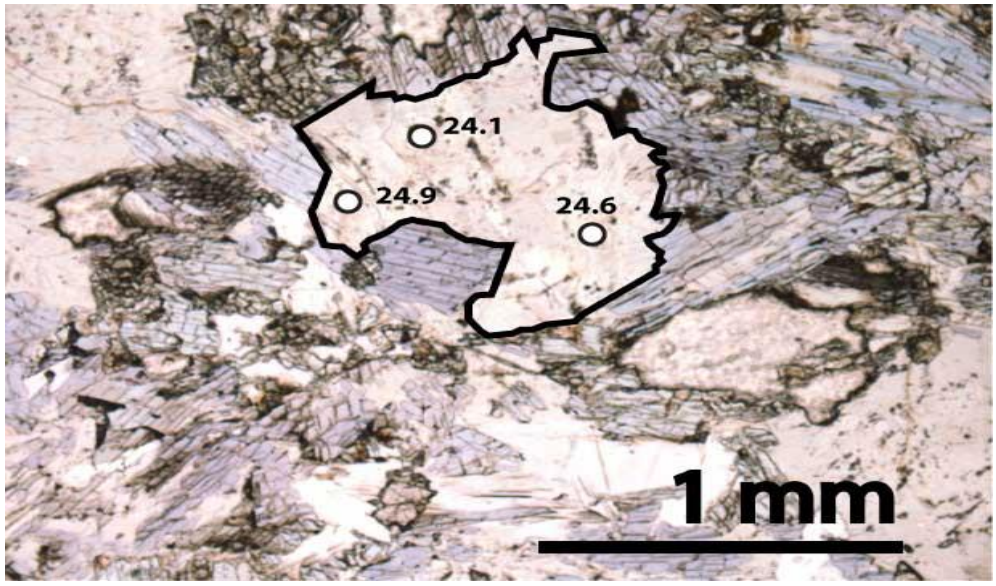

Figure 27: MH90-9 Chlorite 4 5x all Li concentrations ±1.5

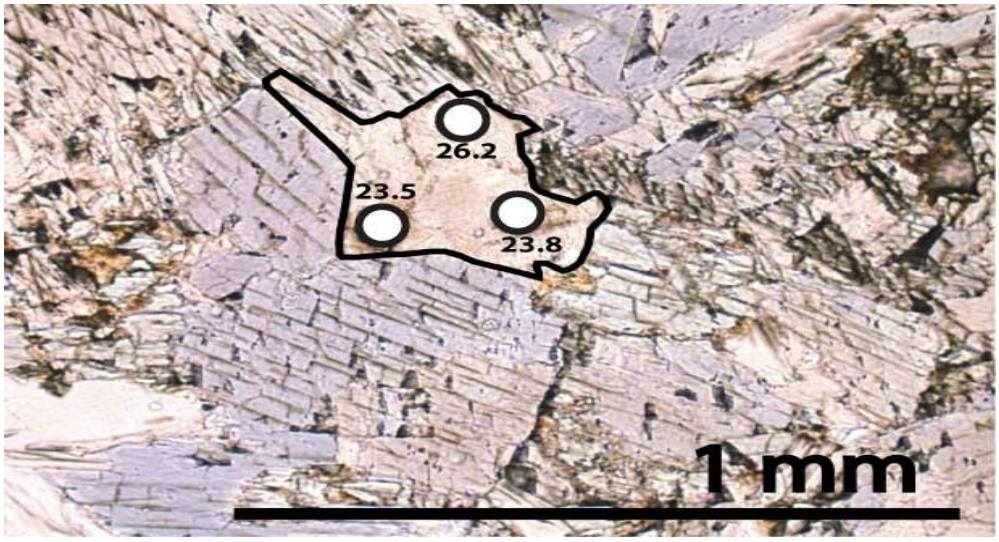

Figure 28: MH90-9 Chlorite 5 10x all Li concentrations ±1.5

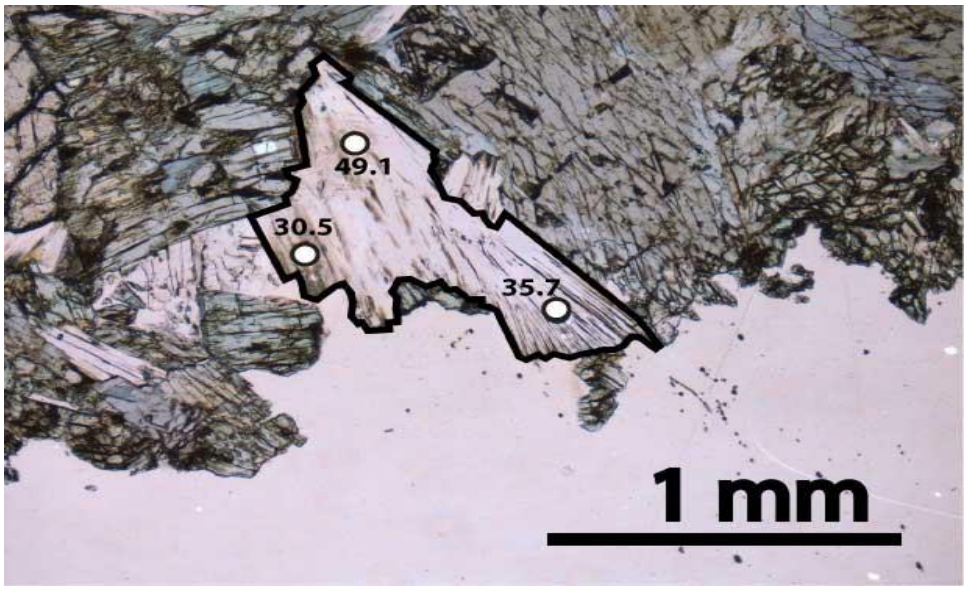

Figure 29: MH90-9 Phengite 1 5x all Li concentrations ±2.5

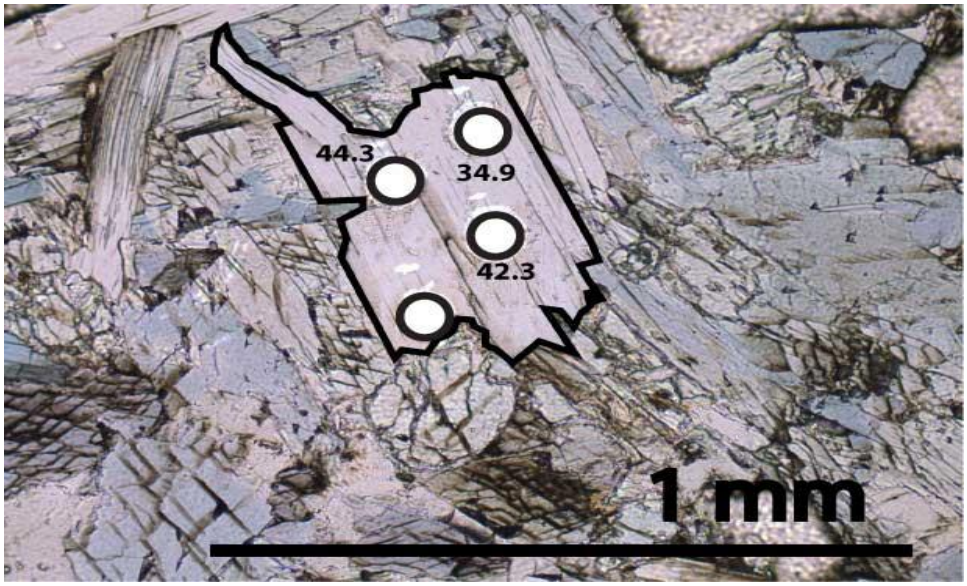

Figure 30: MH90-9 Phengite 2 10x all Li concentrations ±2.5

Figure 31: MH90-9 Phengite 3 10x all Li concentrations ±2.5

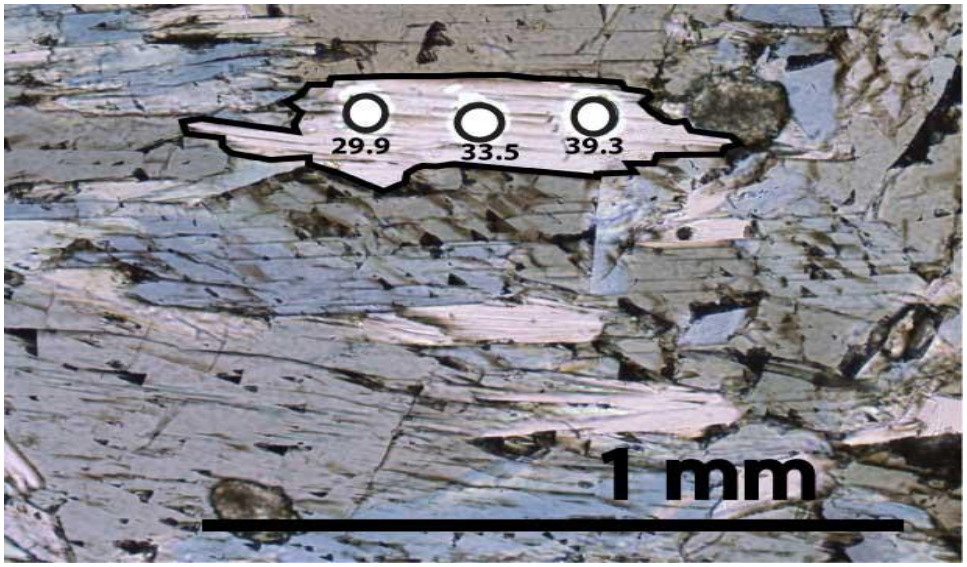

Figure 32: MH90-9 Phengite 4 10x all Li concentrations ±2.5

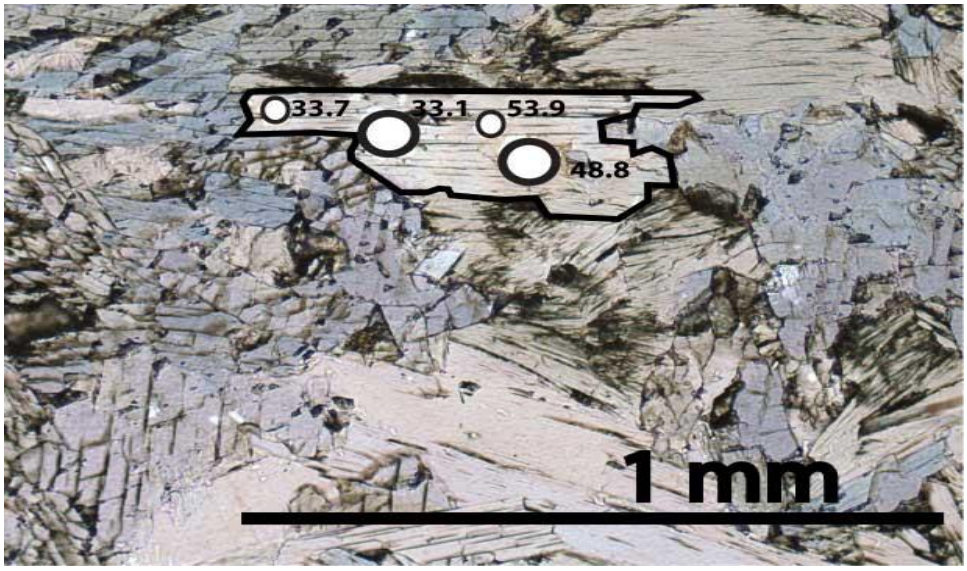

Figure 33: MH90-9 Phengite 5 10x all Li concentrations ±2.5

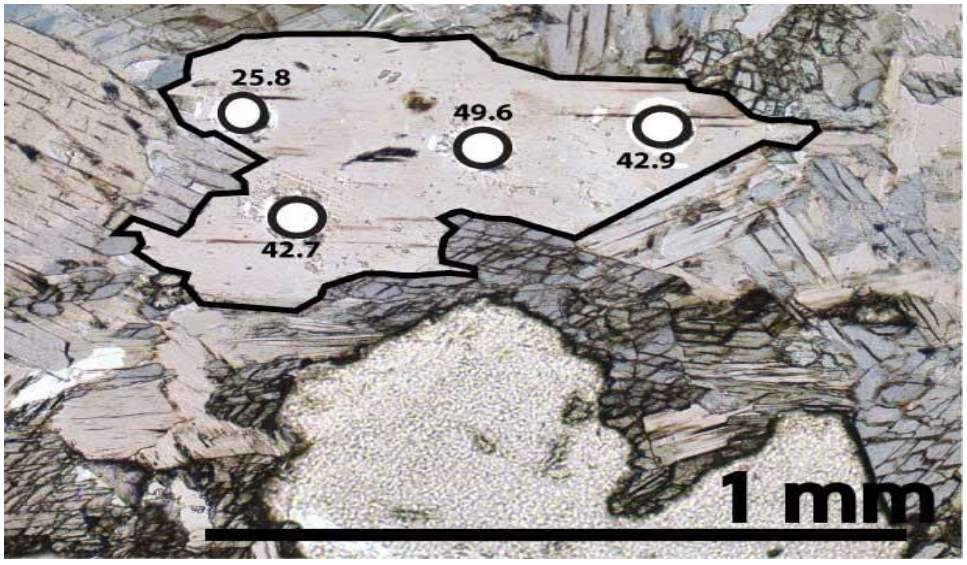

Figure 34: MH90-9 Phengite 6 10x all Li concentrations ±2.5

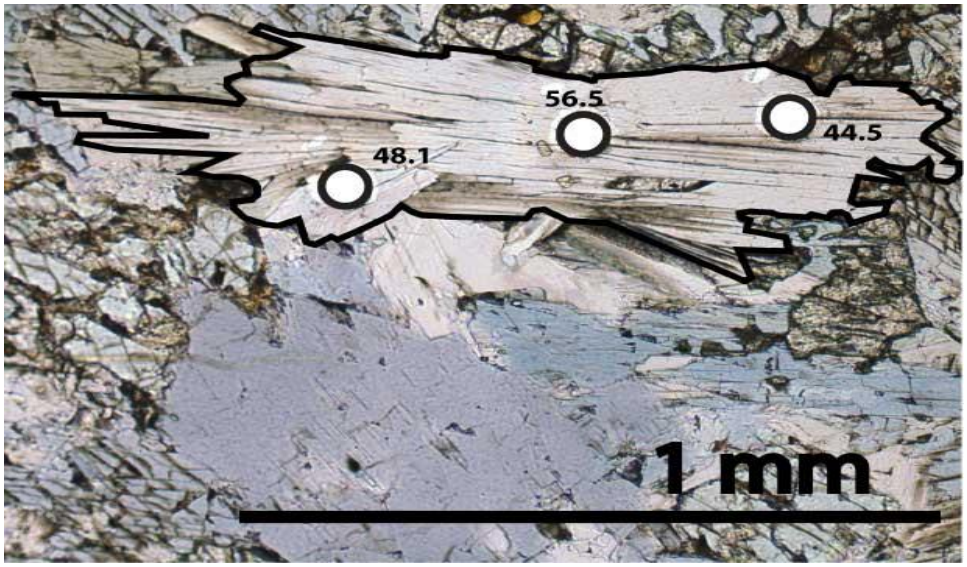

Figure 35: MH90-9 Phengite 7 10x all Li concentrations ±2.5

Block Core

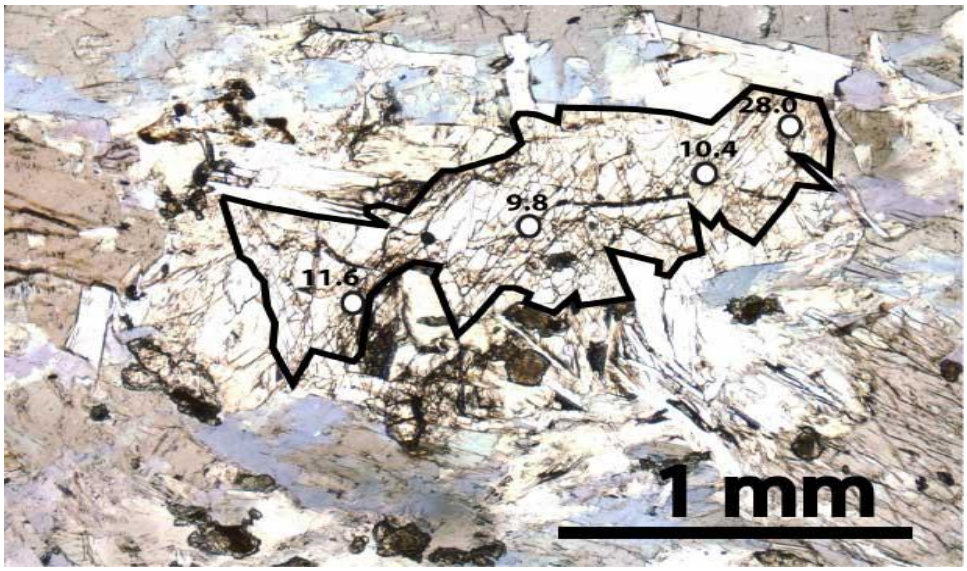

Figure 36: MH90-1Aa Amphibole 1 5x all Li concentrations ±0.8

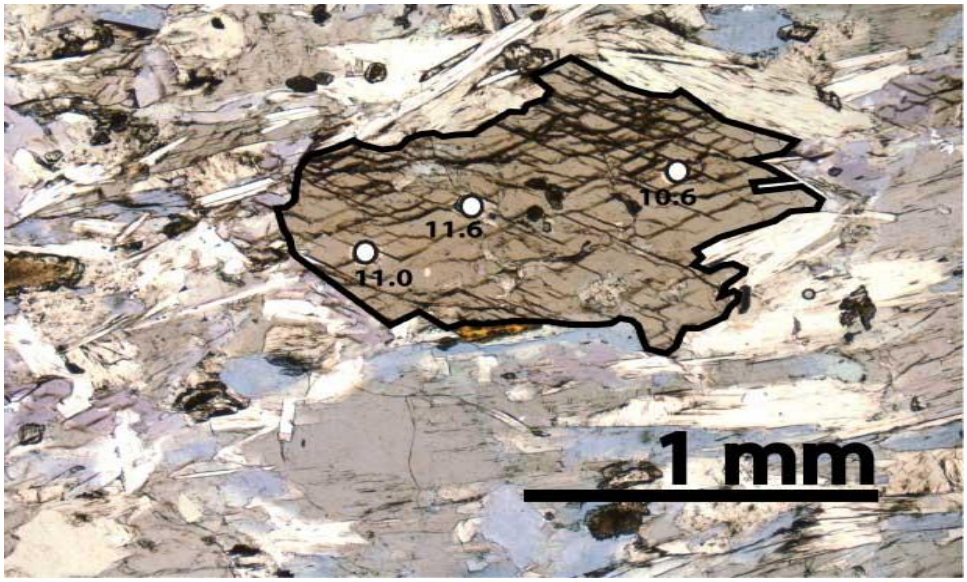

Figure 37: MH90-1Aa Amphibole 2 5x all Li concentrations ±0.8

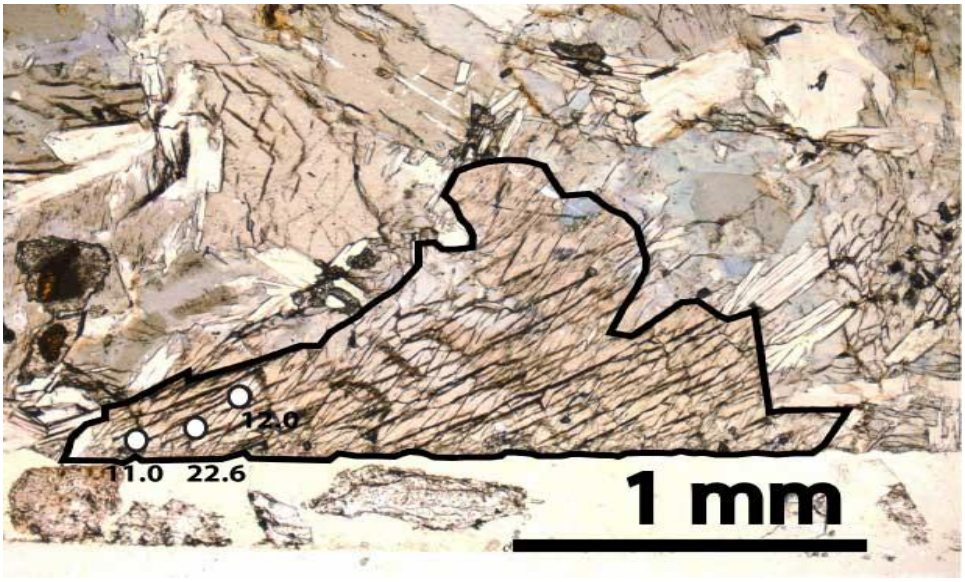

Figure 38: MH90-1Aa Amphibole 3 5x all Li concentrations ±0.8

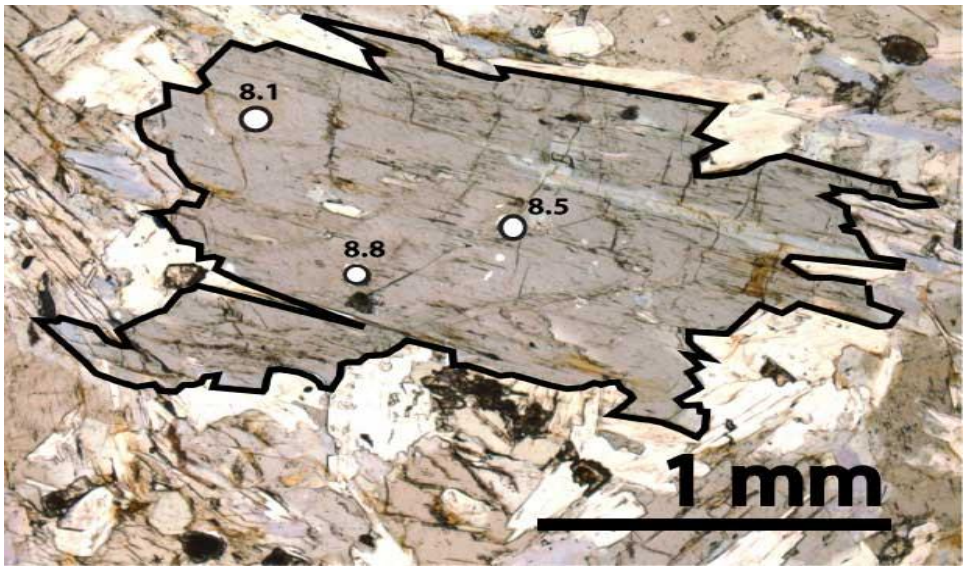

Figure 39: MH90-1Aa Amphibole 4 5x all Li concentrations ±0.8

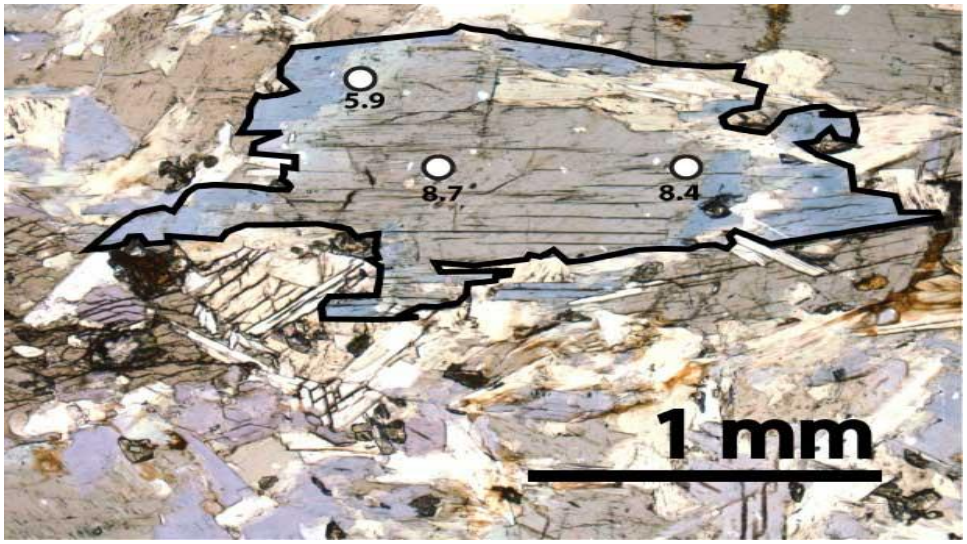

Figure 40: MH90-1Aa Amphibole 5 5x all Li concentrations ±0.8

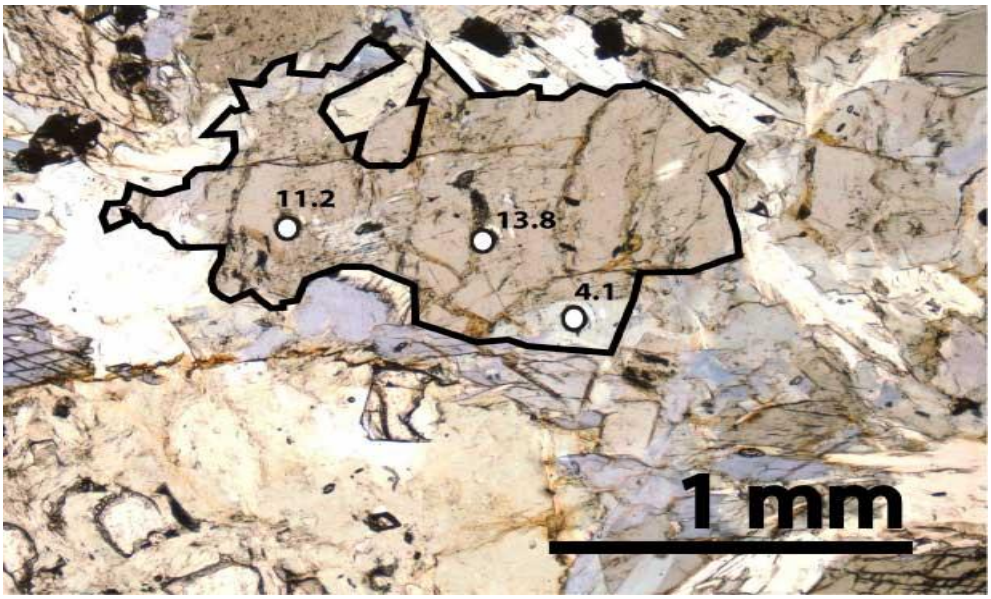

Figure 41: MH90-1Aa Amphibole 6 5x all Li concentrations ±0.8

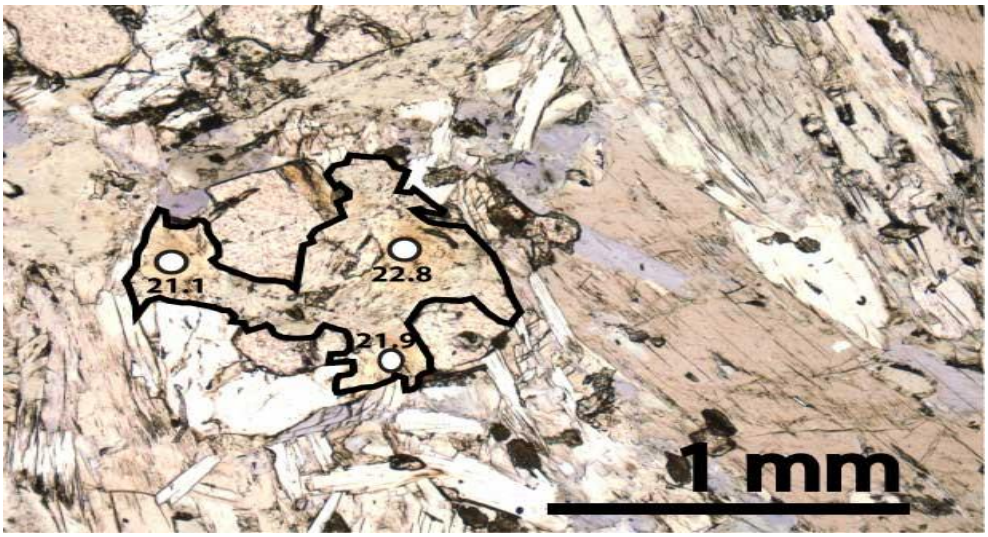

Figure 42: MH90-1Aa Chlorite 1 5x all Li concentrations ±1.4

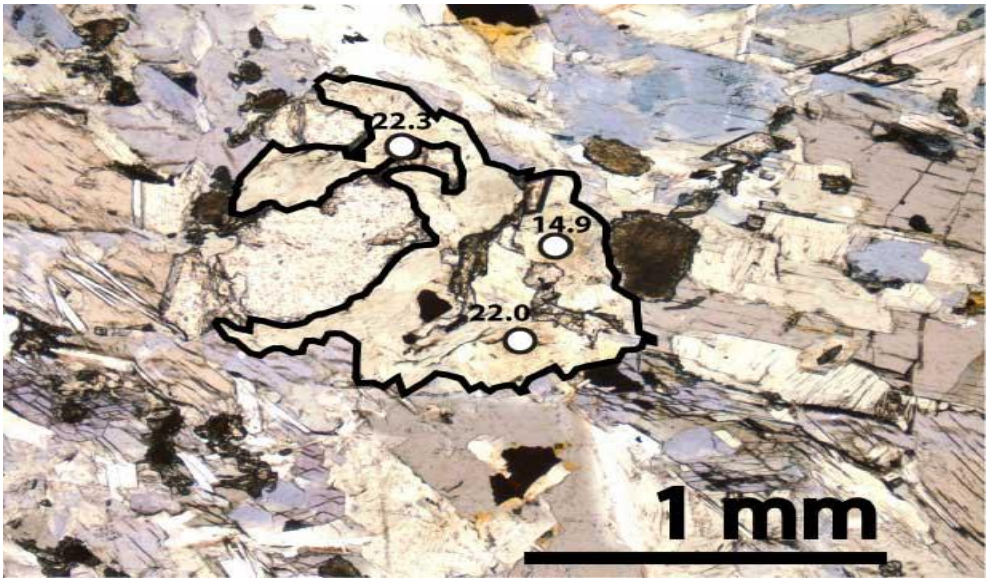

Figure 43: MH90-1Aa Chlorite 2 5x all Li concentrations ±1.4

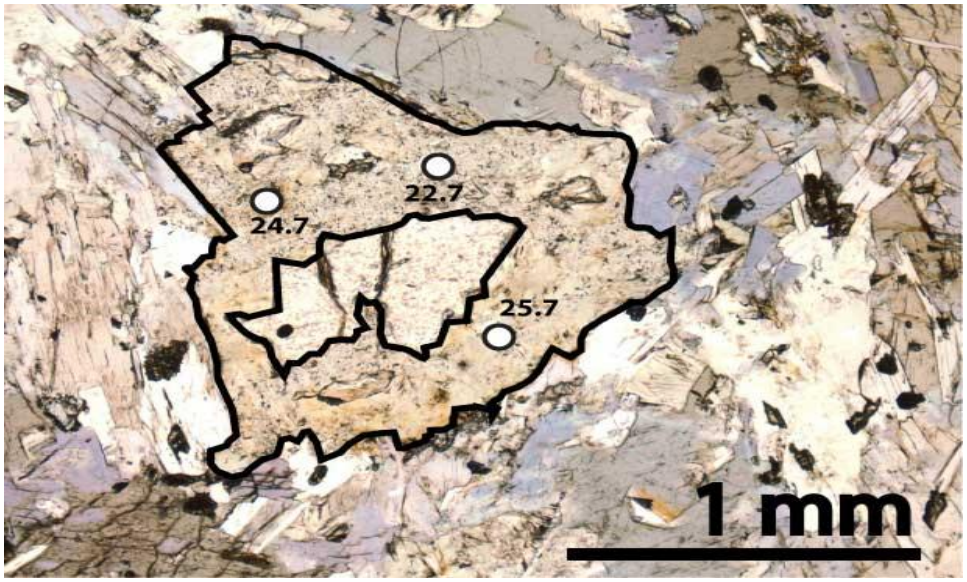

Figure 44: MH90-1Aa Chlorite 4 5x all Li concentrations ±1.4

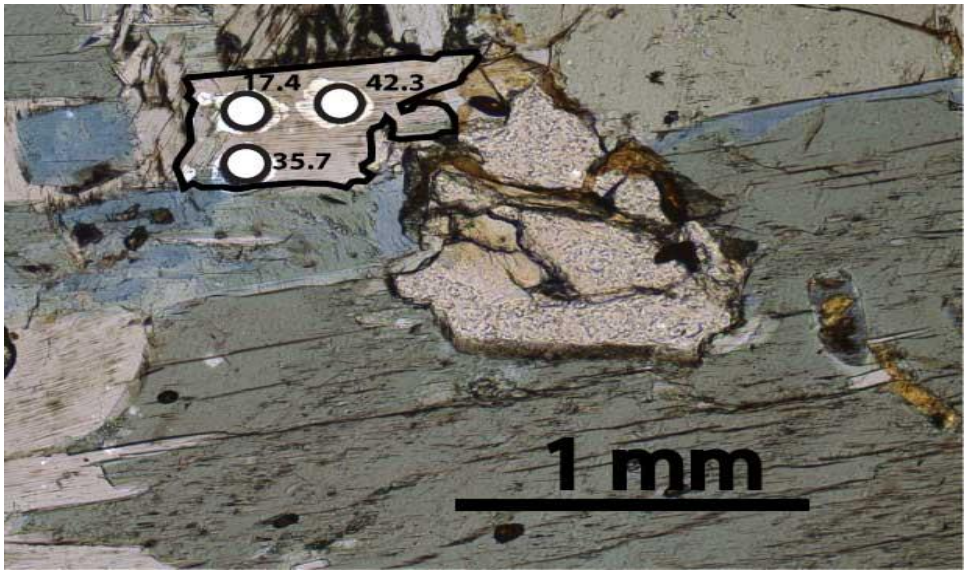

Figure 45: MH90-1Aa Phengite 1 10x all Li concentrations ±2.5

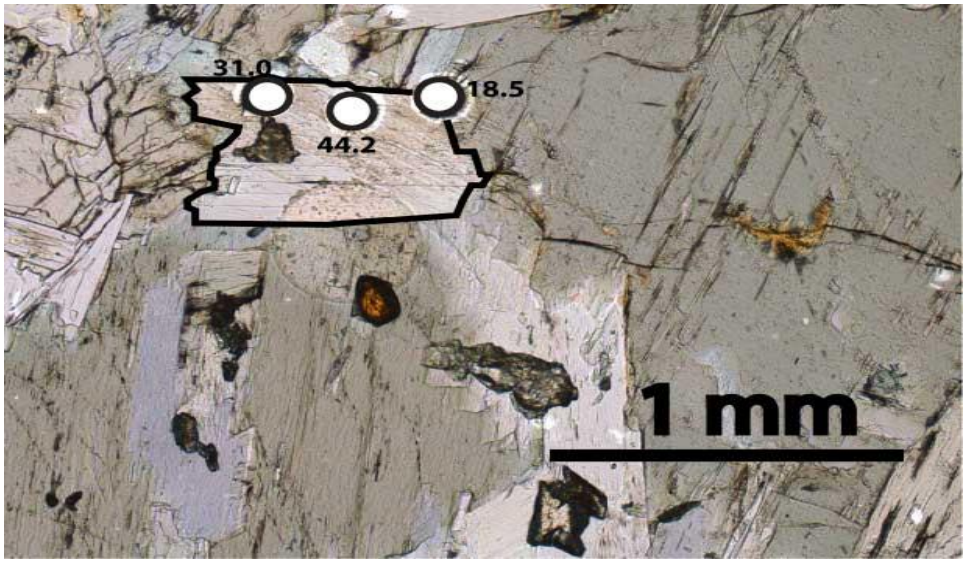

Figure 46: MH90-1Aa Phengite 2 10x all Li concentrations ±2.5

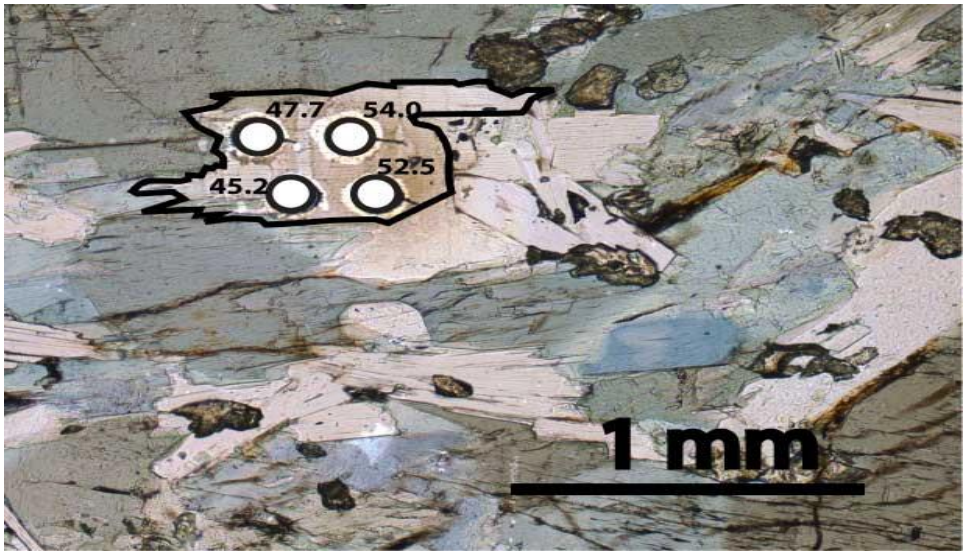

Figure 47: MH90-1Aa Phengite 3 10x all Li concentrations ±2.5

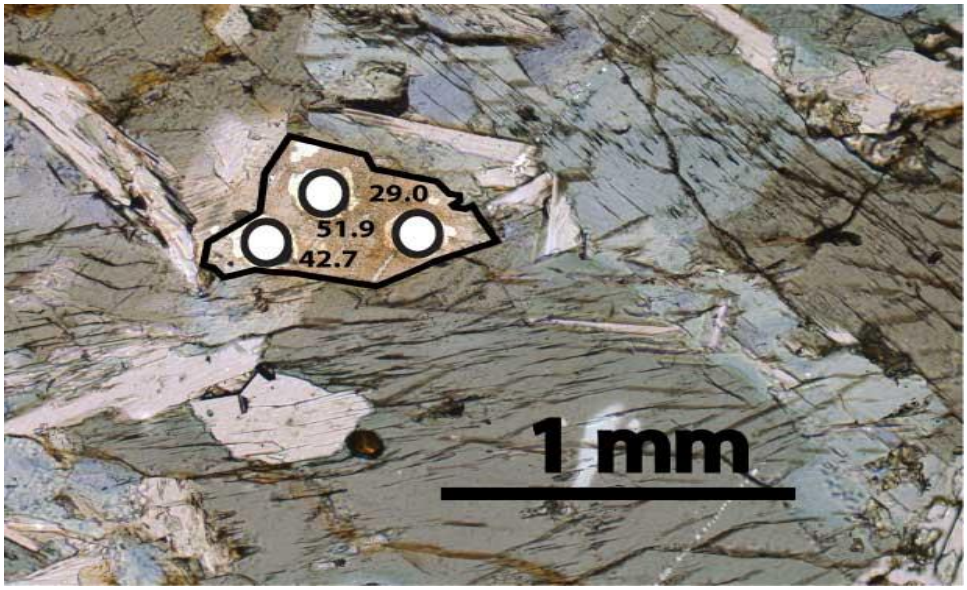

Figure 48: MH90-1Aa Phengite 4 10x all Li concentrations ±2.5

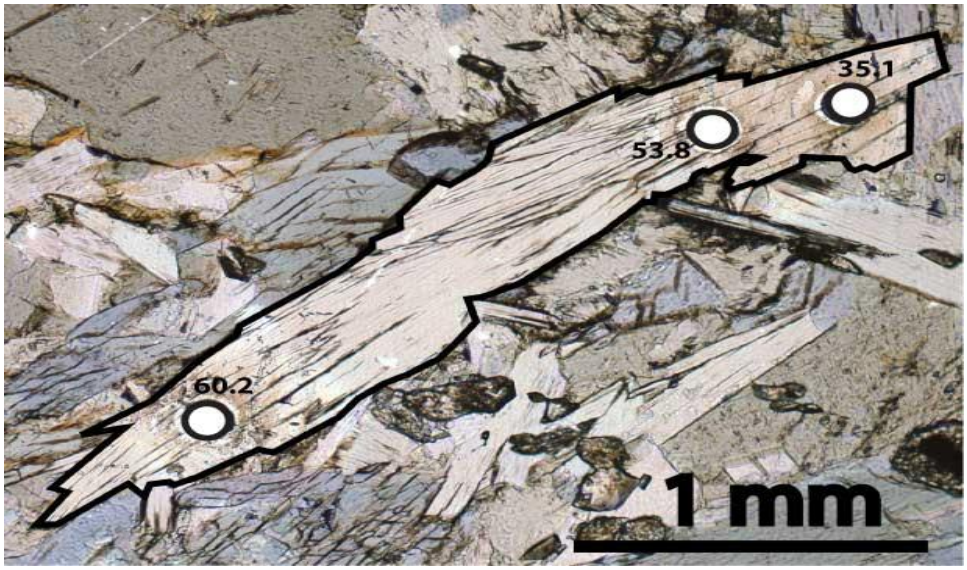

Figure 49: MH90-1Aa Phengite 5 10x all Li concentrations ±2.5

Vein

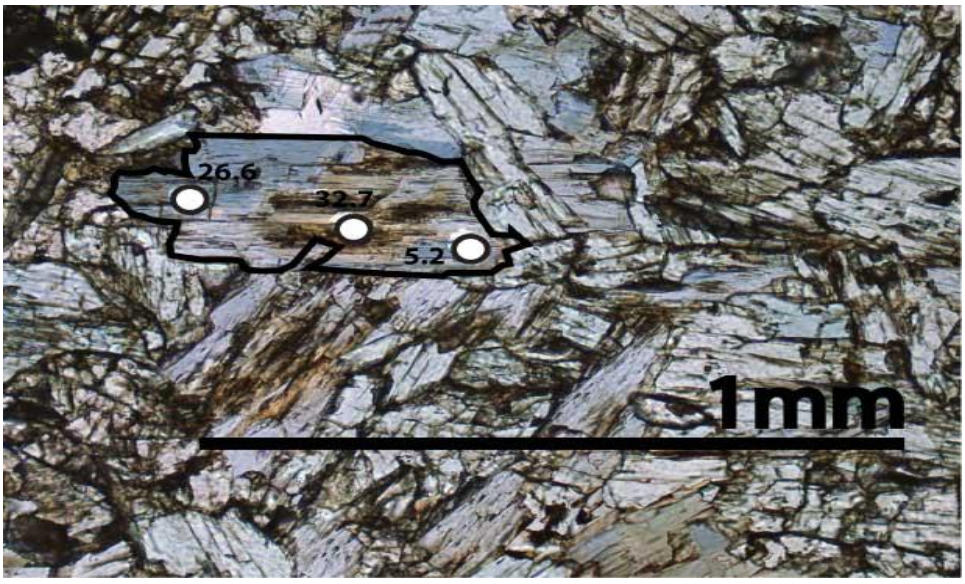

Figure 50: MH90-11c Amphibole 1 10x all Li concentrations ±1.1

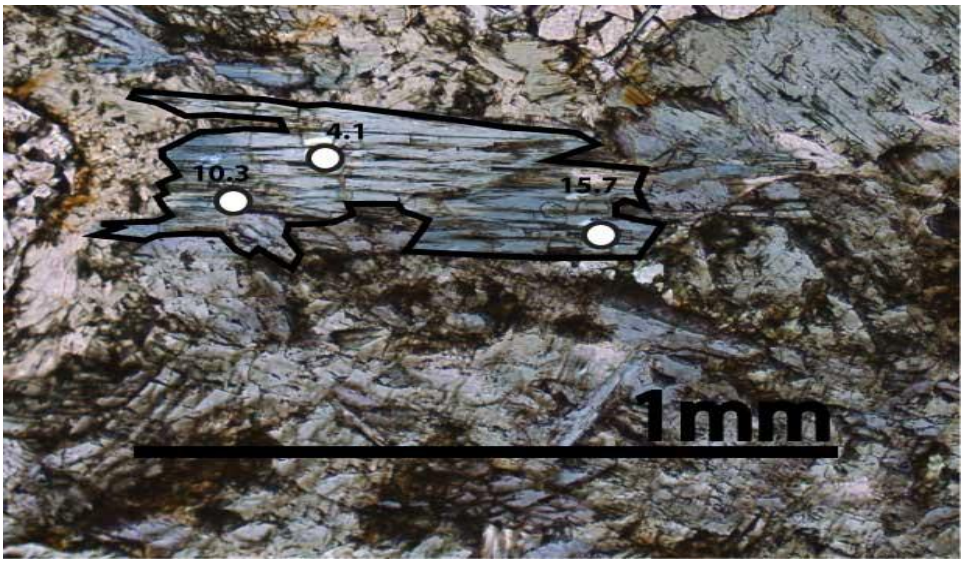

Figure 51: MH90-11c Amphibole 2 10x all Li concentrations ±1.1

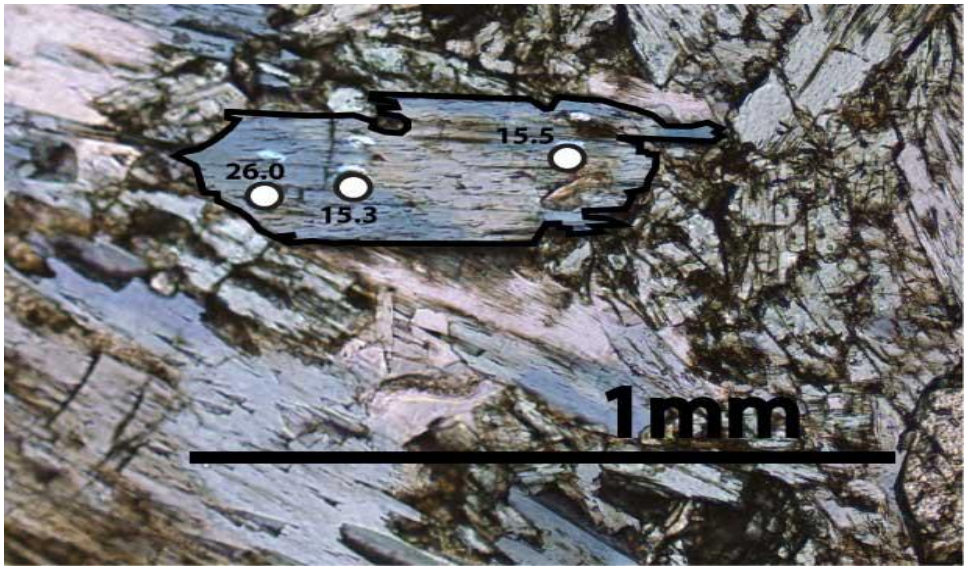

Figure 52: MH90-11c Amphibole 3 10x all Li concentrations ±1.1

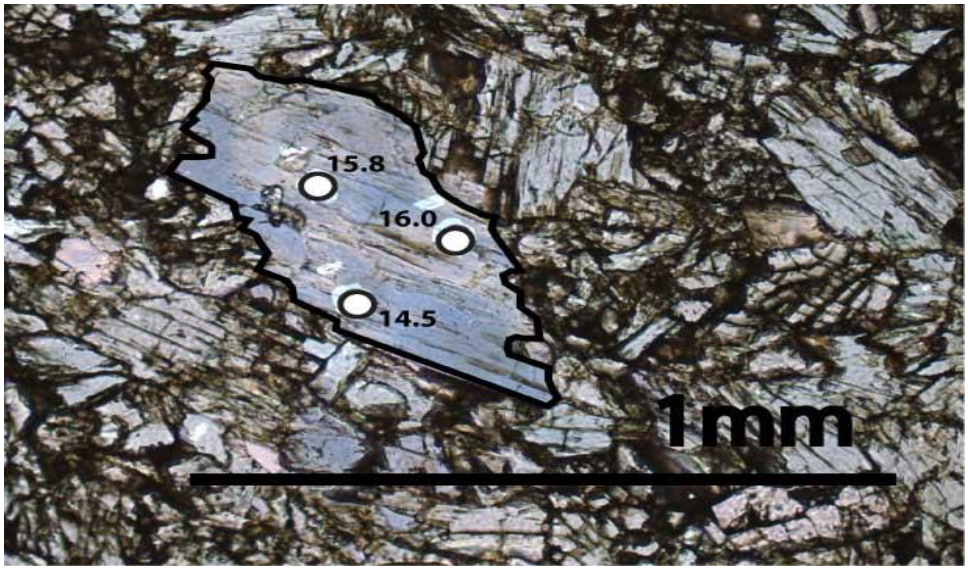

Figure 53: MH90-11c Amphibole 4 10x all Li concentrations ±1.1

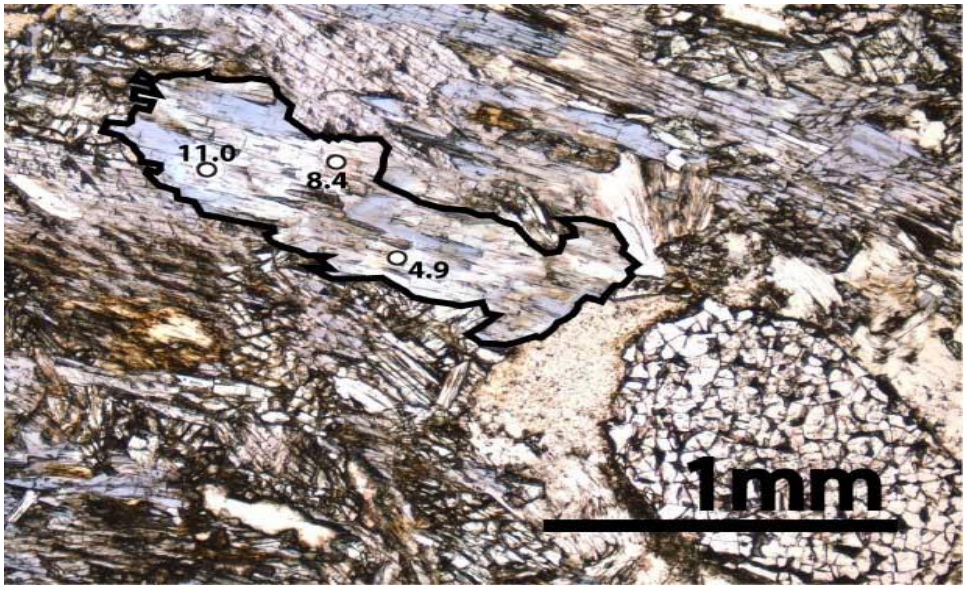

Figure 54: MH90-11c Amphibole 5 5x all Li concentrations ±1.1

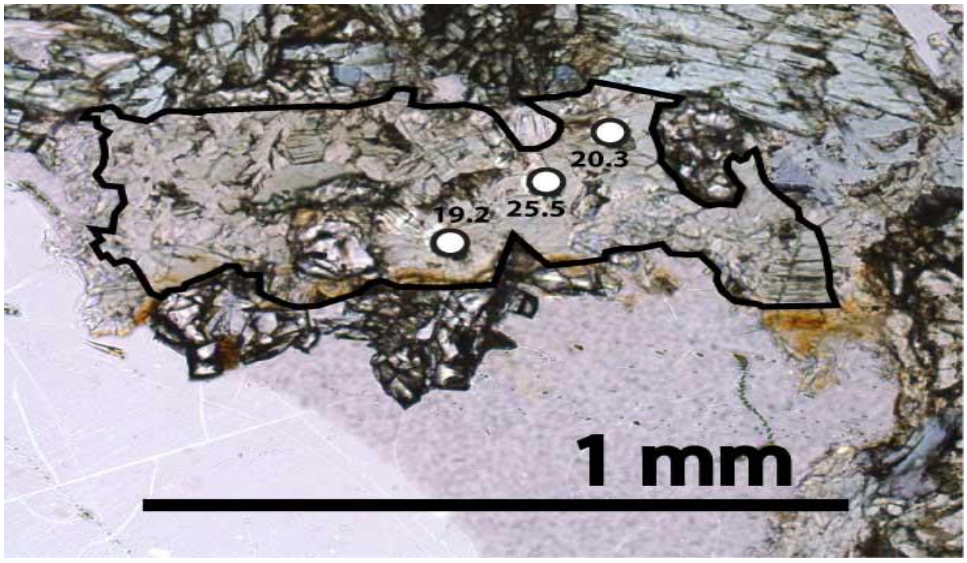

Figure 55: MH90-11c Chlorite 1 10x all Li concentrations ±2.7

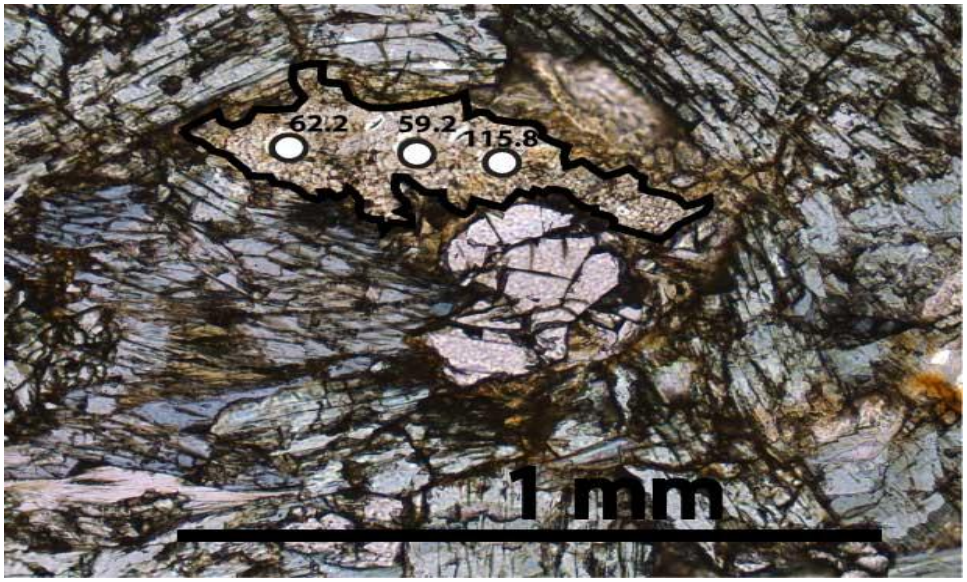

Figure 56: MH90-11c Chlorite 2 10x all Li concentrations ±2.7

Figure 57: MH90-11c Chlorite 3 10x all Li concentrations ±2.7

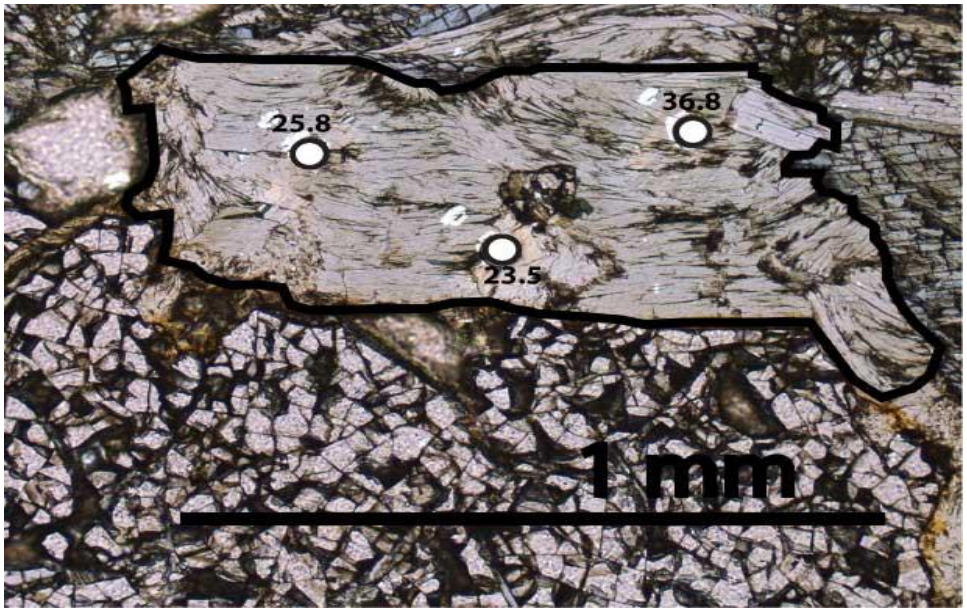

Figure 58: MH90-11c Chlorite 4 10x all Li concentrations ±2.7

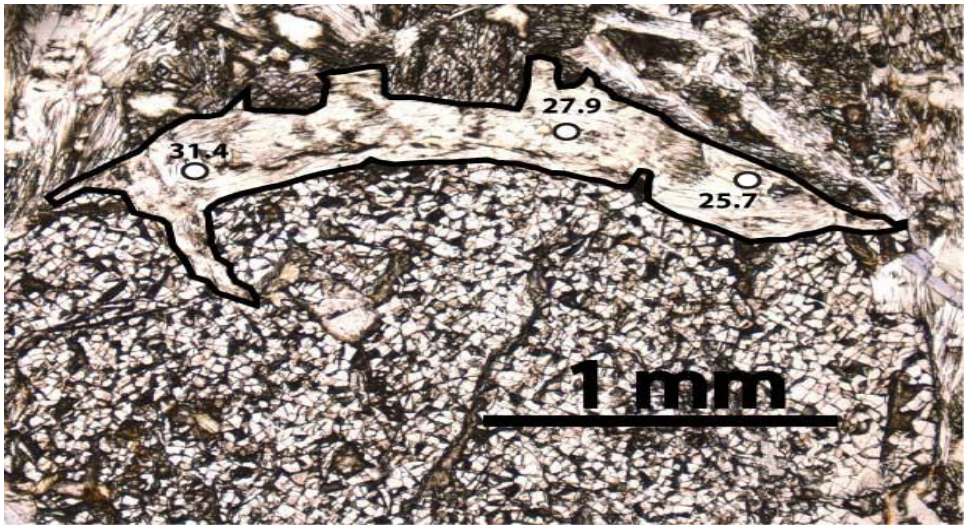

Figure 59: MH90-11c Chlorite 5 5x all Li concentrations ±2.7

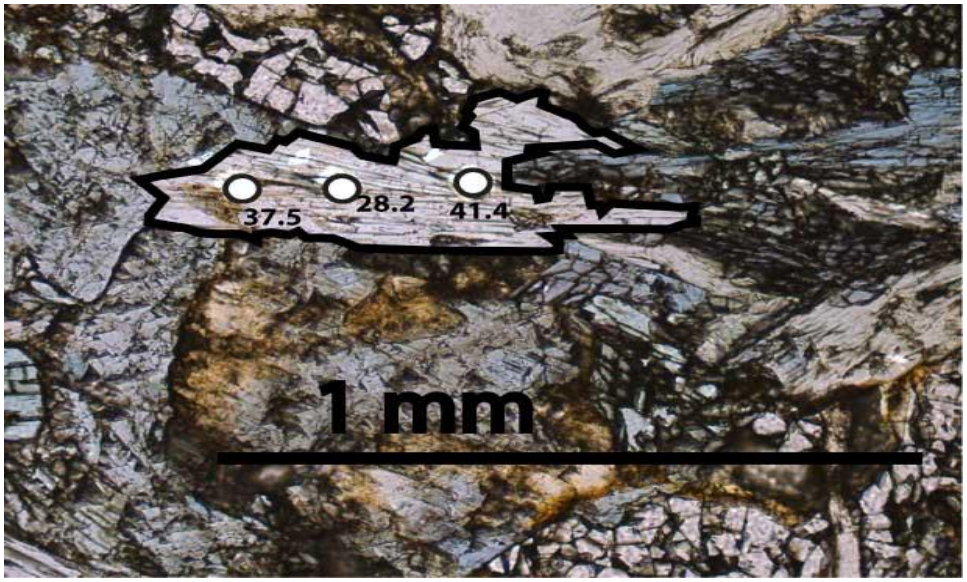

Figure 60: MH90-11c Phengite 1 10x all Li concentrations ±2.2

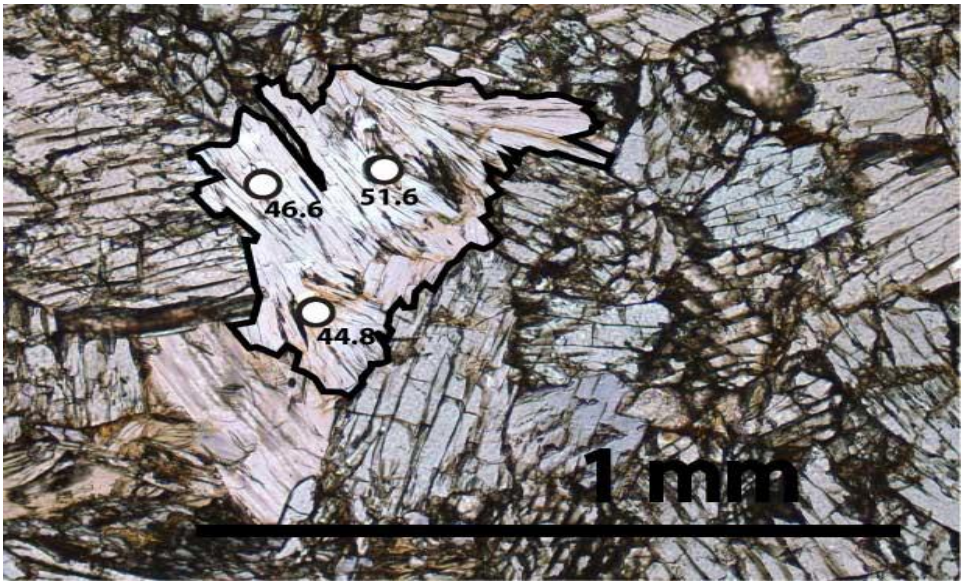

Figure 61: MH90-11c Phengite 2 10x all Li concentrations ±2.2

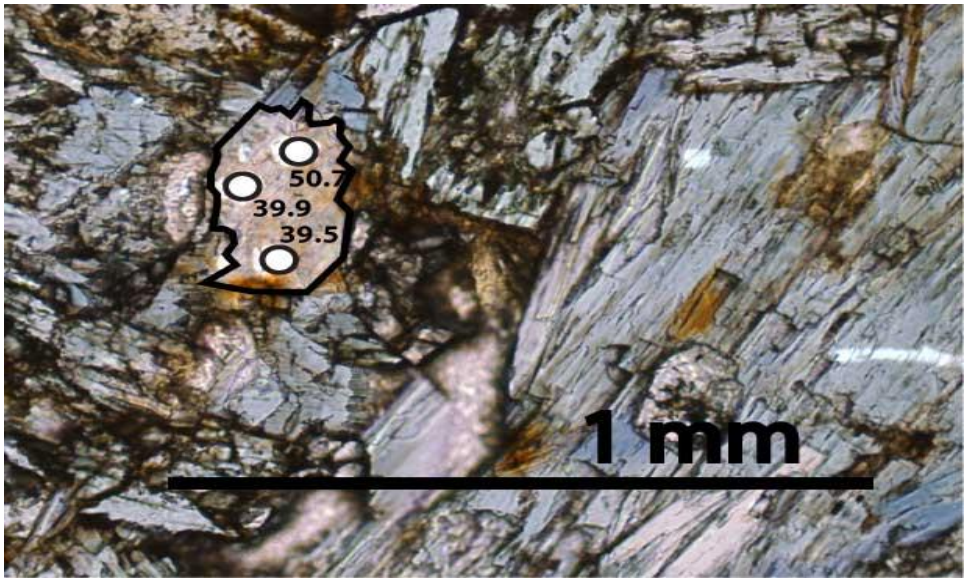

Figure 62: MH90-11c Phengite 3 10x all Li concentrations ±2.2

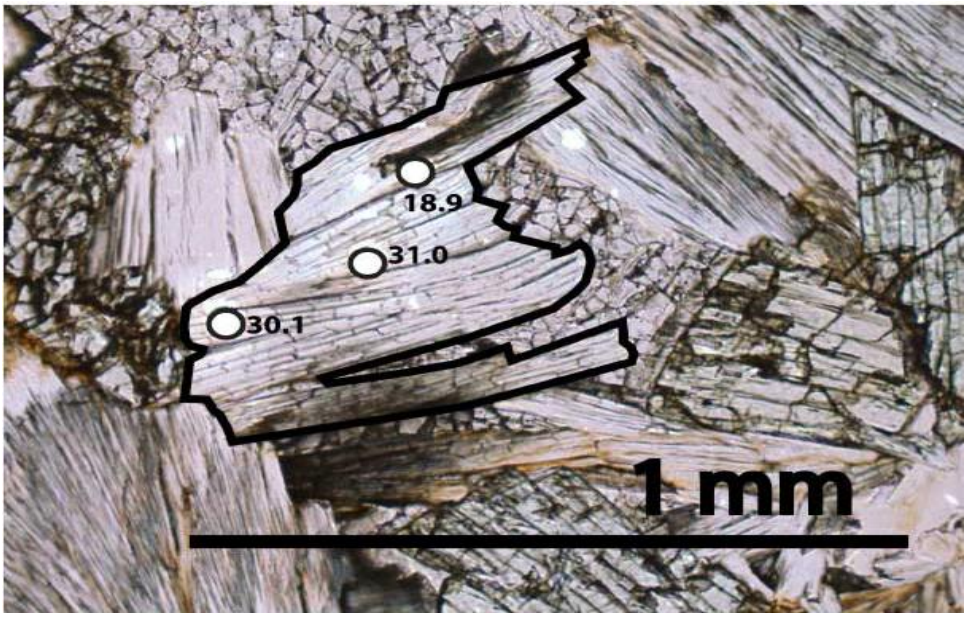

Figure 63: MH90-11c Phengite 4 10x all Li concentrations ±2.2

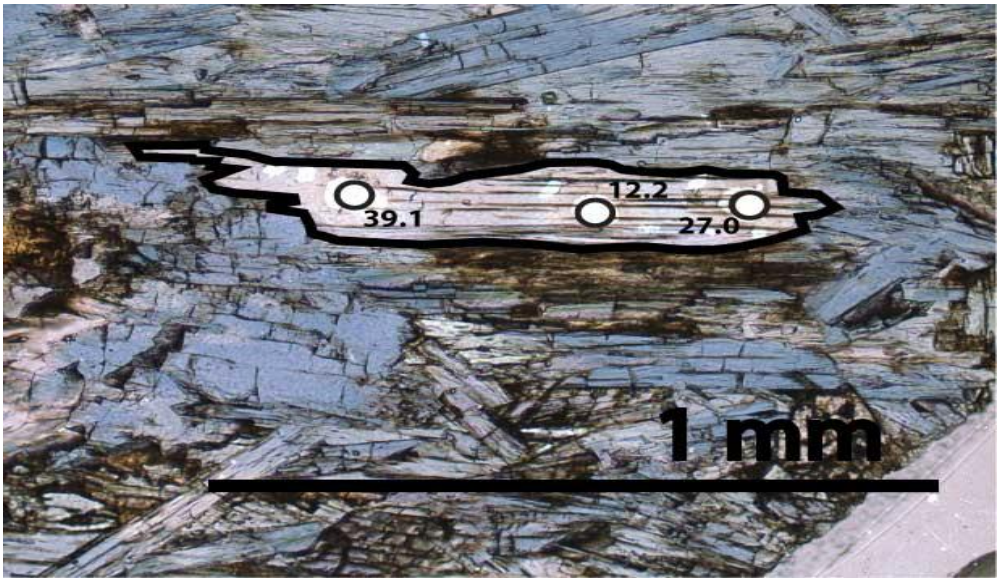

Figure 64: MH90-11c Phengite 5 10x all Li concentrations ±2.2

Appendix 3: Honor Pledge

I pledge on my honor that I have not given or received any unauthorized assistance on this assignment or examination.

Sarah E. Regen

Bibliography

Achterberg, E.V., Ryan, C.G., Jackson, S.E., and Griffin, W.L., 2001. Appendix 3: Data Reduction Software for LA-ICP-MS. In *Laser Ablation-ICP-MS in Earth Sciences* **249**, 243.

Anthony, J.W., Bideaux, R.A., Bladh, K.W.,and Nichols, M.C.. *Handbook of Mineralogy*. Tucson, Arizona: Mineral Data, 1990, 1991. Print.

Bebout, G.E., and Barton, M.D., 1989. Fluid Flow and Metasomatism in Subduction Zone Hydrothermal System: Catalina Schist Terrane, California. *Geology* **17**, 976 – 980.

Bebout, G.E., 2007. Metamorphic Chemical Geodynamics of Subduction Zones. *Earth and Planetary Science Letters* **260**, 373 – 393.

Brandelik, A., 2004. CALCMIN- an EXCEL Visual Basic Application for Calculating Mineral Structure Formulae from Electron Microprobe Analyses. *Computers and Geosciences* **35**, 1540 – 1551.

Breeding, C.M., Ague, J.J., and Brocker, M., 2004. Fluid Metasedimentary Rock Interactions and the Chemical Composition of Arc Magmas. *Geology* **32**, 1041 – 1044.

Brenan J.M., Ryerson, F.J., and Shaw, H.F., 1998. The Role of Aqueous Fluids in the Slab-To-Mantle Transfer of Boron, Beryllium, and Lithium During Subduction: Experiments and Models. *Geochimica et Cosmochimica Acta* **62**, 3337 – 3347.

Brigatti, M.F., Kile, D.E., Poppi, M., 2001. Crystal Structure and Crystal Chemistry of Lithium-Bearing Muscovite-2M_1. *The Canadian Mineralogist* **39**, 1171 – 1180.

Catlos, E.J. and Sorensen, S.S., 2003. Phengite Based Chronology of K- and Ba- Rich Fluid Flow in Two Paleosubduction Zones. *Science* **299**, 92 – 95.

Chan, L.H., Alt, J.C., and Teagle, D.A.H., 2002. Lithium and Lithium Isotope Profiles Through the Upper Oceanic Crust: A Study of Seawater-Basalt Exchange at ODP Sites 540B and 896A. *Earth and Planetary Science Letters* **201**, 187 – 201.

Cibin, G., G. Cinque, A. Marcelli, A. Mottana, & R. Sassi (2008): The octahedral sheet of metamorphic 2M1-phengites: a combined EMPA and AXANES study: American Mineralogist **93**, 414-425. .

Cloos, M., 1986. Blueschists in the Franciscan Complex of California: Petrotectonic Constraints on uplift Mechanisms. *Geological Society of America, Memoir* **164**, 77 - 93.

Coleman, R.G. & Lanphere, M.A., 1971. Distribution and Age of High-Grade Blueschists, Associated Eclogites, and Amphibolites from Oregon and California. *Geological Society of America Bulletin* **82,** 2397- 2412.

Cowan, D.S., 1974. Deformation and Metamorphism of the Franciscan Subduction Zone Complex Northwest of Pacheco Pass, California. *Geological Society of America* **85,** 1623 – 1634

Deer, William Alexander., Robert Andrew. Howie, and Jack Zussman. *Rock Forming Minerals.* Ann Arbor (Mich.): UMI, 1995. Print.

Esawi, E.K., 2004, AMPH-CLASS: An Excel spreadsheet for the classification and nomenclature of amphiboles based on the 1997 recommendations of the International Mineralogical Association: Computers and Geosciences, 30, **7**, 753-760.

GeoReM <http://georem.mpch-mainz.gwdg.de/>

Giaramata, M.J. & Sorensen, S.S., 1994. Primary Fluids in Low- Temperature Eclogites: Evidence from two Subduction Complexes (Dominican Republic, and California, USA). *Contributions to Mineralogy and Petrology* **117**, 279 – 292.

Hawthorne, F.C., and Oberti, R., 2007. Classification of Amphiboles. *Reviews in Mineralogy and Geochemistry* **67**, 55 – 88.

Herrington, K. L., 1985. Metamorphism, Deformation and Metasomatic Alteration of an Eclogite Block in the Franciscan Subduction Complex, Near Mt. Hamilton, Central Diablo Range, California. *Thesis, University of Austin*.

Krough, E.J., Oh, C.W., and Liou, J.G., 1994. Polyphase and Anticlockwise P-T evolution for Franciscan Eclogites and Blueschists from Jenner, California, USA. *Journal of Metamorphic Geology* **12**, 121 – 134.

Marschall, H.R., Pogge von Strandmann, P.A.E., Seitz, H-M., Elliott, T., and Niu, Y., 2007. The Lithium Isotopic Composition of Orogenic Eclogites and Deep Subducted Slabs. *Earth and Planetary Science Letters* **262**, 563 – 580.

Moore, D.E. and Blake, M.C., Jr, 1989. New Evidence for Polyphase Metamorphism of Glaucophane Schist and Eclogite Exotic Blocks in the Franciscan Complex, California and Oregon. *Journal of Metamorphic Geology* **7**, 192 – 211.

Moore, D.E., 1984. Metamorphic History of a High-Grade Blueschist Exotic Block from the Franciscan Complex, California. *Journal of Petrology* **25**, 126 – 150.

Nelson, B.K., 1995. Fluid-Flow in Subduction Zones- Evidence from Nd and Sr- Isotope Variations in Metabasalts of the Franciscan Complex, California. *Contributions to Mineralogy and Petrology* **119**, 247 – 262.

Penniston–Dorland, S.C., Sorensen, S.S., Ash, R.D., and Khadke, S.V., 2010. Lithium Isotopes as a Tracer of Fluids in a Subduction Zone Mélange: Franciscan Complex, CA. *Earth and Planetary Science* **292**, 181-190.

Philpotts, A.R., and Ague, J.J., 2009. *Principles of Igneous and Metamorphic Petrology.* Cambridge University Press.

Potts, P.J., 1987. *A Handbook of Silicate Rock Analysis*. Chapman and Hall.

Sorensen, S.S. and Grossman, J.N., 1989. Enrichment of Trace Elements in Garnet-Amphibolites from a Paleo-Subduction Zone: Catalina Schist, Southern California. *Geochemica et Cosmochemica Acta* **53**, 3155 – 3177.

Sorensen, S.S. and Grossman, J.N. and Perfit, M.R., 1997. Phengite- Hosted LILE Enrichment in Eclogite and Related Rocks: Implications for Fluid- Mediated Mass Transfer in Subduction Zones and Arc Magma Genesis. *Journal of Petrology* **38**, 3 – 34.

Spear, F.S., 1993. *Metamorphic Phase Equilbria and Pressure-Temperature-Time Paths.* Mineralogical Society of America.

Tatsumi, Y., 2005. The Subduction Factory: How it Operates in the Evolving Earth. *Geological Society of America Today* **15,** 4 – 10.

Wakabayashi, J., 1990. Counterclockwise P-T-t Paths from Amphibolites, Franciscan Complex, California: Relics from the Early Stages of Subduction Zone Metamorphism. *Journal of Geology* **98**, 657 – 680.

Winter, John D. *An Introduction to Igneous and Metamorphic Petrology*. New York, NY: Prentice Hall, 2010. Print.

Wunder, B., Meixner, A., Romer, R.L., Feenstra, A., Schettler, G., Heinrich, W., 2007. Lithium Isotope Fractionation Between Li- bearing Staurolite, Li-mica and Aqueous Fluids: An Experimental Study. *Chemical Geology* **238**, 277 – 290.

Zack, T., Tomascak, P.B., Rudnick, R.L., Dalpe, C., and McDonough, W.F., 2003. Extremely Light Lithium in Orogenic Eclogites: The Role of Isotope Fractionation During Dehydration in Subducted Oceanic Crust. *Earth and Planetary Science Letters* **208**, 279 – 290.